Measurement of the Reynolds stresses and the mean-flow field in a three-dimensional pressure-driven boundary layer

By UDO R. MÜLLER

Aerodynamisches Institut, Technische Hochschule Aachen, West Germany

An experimental study of a steady, incompressible, three-dimensional turbulent boundary layer approaching separation is reported. The flow field external to the boundary layer was deflected laterally by turning vanes so that streamwise flow deceleration occurred simultaneous with cross-flow acceleration. At 21 stations profiles of the mean-velocity components and of the six Reynolds stresses were measured with single- and X-hot-wire probes, which were rotatable around their longitudinal axes. The calibration of the hot wires with respect to magnitude and direction of the velocity vector as well as the method of evaluating the Reynolds stresses from the measured data are described in a separate paper (Müller 1982, hereinafter referred to as II). At each measuring station the wall shear stress was inferred from a Preston-tube measurement as well as from a Clauser chart. With the measured profiles of the mean velocities and of the Reynolds stresses several assumptions used for turbulence modelling were checked for their validity in this flow. For example, eddy viscosities for both tangential directions and the corresponding mixing lengths as well as the ratio of resultant turbulent shear stress to turbulent kinetic energy were derived from the data.

1. Introduction

Present and future problems in fluid mechanics require prediction methods for three-dimensional turbulent boundary-layer flows. One significant item for the development of reliable computational methods is the improved understanding of turbulent motions (Chapman 1980). Since a general model describing the turbulent momentum and energy transfer is not yet available, empirically fitted models will still have to be used to describe the time-averaged turbulent flows. These models are usually limited to a special class of flows, but are expected to be valid at least over a range of flow conditions. At the Euromech 60 meeting held at Trondheim in 1975, the results of several prediction methods were compared with mean velocities, wall shear stresses and integral profile parameters measured in three-dimensional turbulent boundary layers (see East 1975; Fannelop & Krogstad 1975). With either first-order or second-order closure assumptions fully three-dimensional flows could not be simulated with sufficient accuracy. Additionally Krause & Kordulla showed (see also Krause 1974), using the implicit finite-difference method of Krause, Hirschel & Bothmann (1969) and Krause, Hirschel & Kordulla (1976), that the calculated results depended not only on the choice of closure assumption (algebraic turbulence models), but also on the numerical accuracy. With
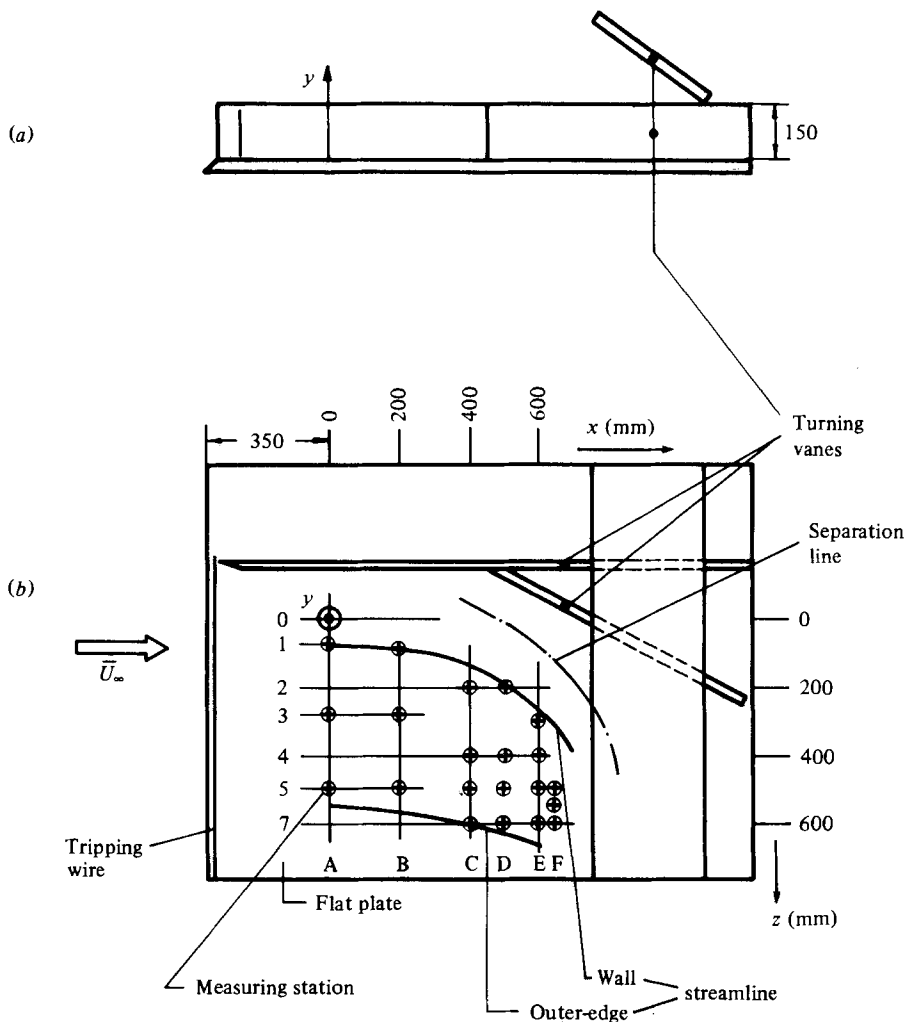
FIGURE 1. Schematic of experimental set up and indication of
measuring stations: (a) side view; (b) top view.

a fourth-order accurate method the simulation of the experiment of van den Berg &
Elsenaar (1972) and Elsenaar & Boelsma (1974) (see also van den Berg *et al.* 1975)
predicted wall shear stresses as much as 15% lower than those obtained with a second-
order method. Compared with the experimental data, both calculations yielded larger
mean velocities and smaller turning angles in the near-wall region of the fully three-
dimensional flow, thus indicating an overestimated momentum transfer towards the
wall by the Reynolds shear stresses.

A major reason for the discrepancies between experiment and numerical simulations
is the insufficient understanding of the mean-flow field and the turbulence structure of
three-dimensional boundary layers. Bradshaw (1972) and Fannelop & Krogstad (1975)
expected to gain more insight into the turbulent momentum transfer from further
detailed experimental investigations. Many experiments have already contributed to
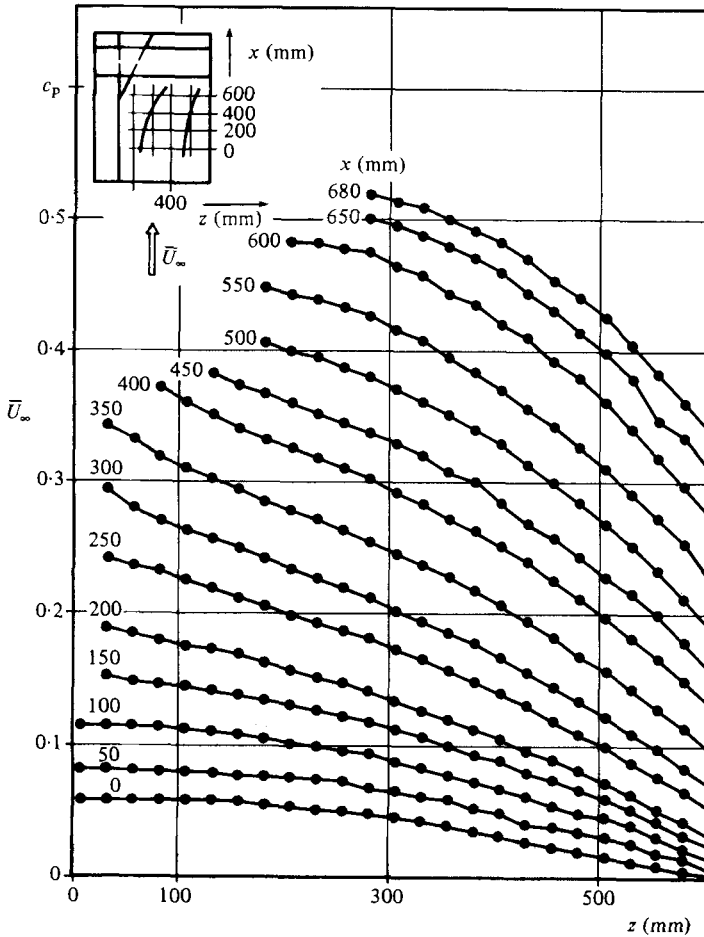our current ideas about three-dimensional pressure-driven turbulent boundary layers.

FIGURE 2. Measured pressure distribution.

For example, the boundary layer approaching a cylinder standing perpendicularly on a wall was investigated by Hornung & Joubert (1963), East & Hoxey (1969), Krogstad (1979) and Dechow (1977) (see also Dechow & Felsch 1977). Three-dimensional turbulent boundary layers with non-zero pressure gradients were also investigated by Johnston (1960), Pierce & Ekzewe (1974) and Pierce & Duerson (1975); these flow fields were created by impinging a two-dimensional flow on a wall perpendicular to the stream axis, thus deflecting the flow laterally. Measurements in quasi-two-dimensional flows, dependent on two space co-ordinates only, were carried out by van den Berg & Elsenaar (1972) and Elsenaar & Boelsma (1974), who investigated a boundary layer with adverse pressure gradients leading to separation, and Johnston (1970), who investigated a flow approaching a swept, forward-facing step. However, there is a need for three-dimensional turbulent boundary-layer experiments that are amenable to numerical simulation and that provide detailed and accurate data suitable for both checking mean-momentum balance and the validity of turbulence models. The present investigation was intended to meet these requirements. In a three-dimensional boundary layer the Reynolds stresses and the mean flow field as well as the wall shear stresses were measured, and the pressure distribution was mapped at the outer edge of the boundary layer.
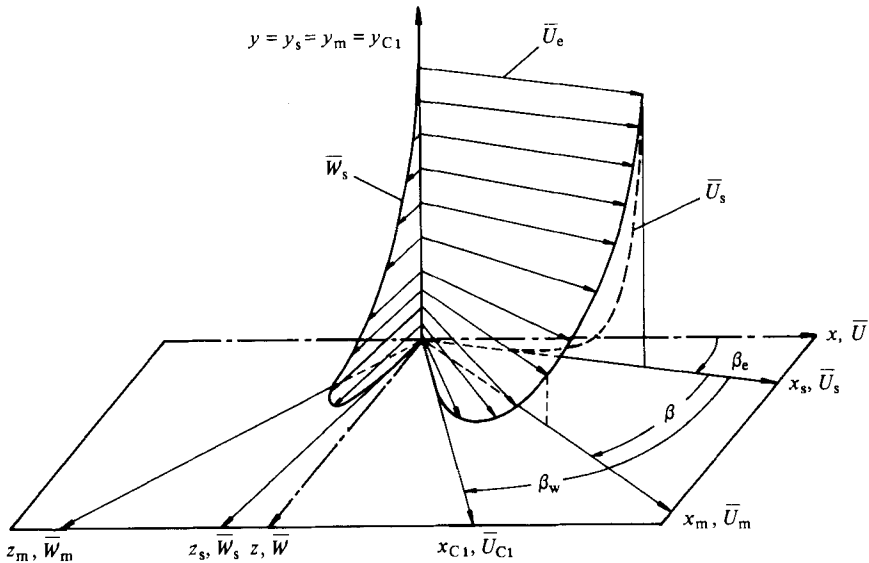
FIGURE 3. Sketch of velocity profiles and definition of co-ordinate systems used.

2. Description of the experiment

2.1. *Experimental setup and measurement technique*

The experiment was carried out in the three-dimensional turbulent boundary layer on a plane smooth Plexiglass plate placed vertically in the open test section (length 1·6 m, diameter 1·2 m) of the return-circuit low-speed wind tunnel of the Aero-dynamisches Institut. The plate was fixed and adjusted with triangular supports on the back side. The free stream was deflected laterally by means of turning vanes as illustrated in figure 1, resulting in turning angles up to 20° compared with the initial flow direction. Thereby a pressure distribution as displayed in figure 2 was imposed on the boundary-layer flow, and caused the wall streamlines to turn up to 50°. Velocity profiles typical for this pressure-driven three-dimensional boundary layer are sketched in figure 3, as well as co-ordinate systems used later. In figure 1, two streamlines determined by numerous hot-wire measurements in the vicinity of the wall and in the outer-edge flow are shown which include the flow field under investigation. The measuring stations covering the attached flow region are marked by crosses. The boundary-layer thickness was artificially increased by tripping the flow with a wire of 5 mm diameter attached to the tapered leading edge with tape. The unit Reynolds number $\overline{U}_\infty/\nu$ was $1\cdot95 \times 10^6\,\mathrm{m}^{-1}$.

The measurements were carried out with a goose-neck-shaped probe support suggested by Johnston (1970) and also used by Dechow (1977) (figures 4 and 5). It could be moved normal to the wall and could be aligned with the local yaw direction while the tip of the probe stayed on the y-axis. Single- and X-hot-wire probes as well as pressure probes could be inserted. Because measuring the complete Reynolds stress tensor required the hot-wire probes to be rotated around their longitudinal axes, the probe support allowed a 360° rotation in intervals of 45°. Additionally it was inclined at a fixed angle $\epsilon_0 = 10°$ with respect to the wall for carrying out near-wall measurements. The angle ϵ_0 and the distance y from the wall were adjusted with a mechanical
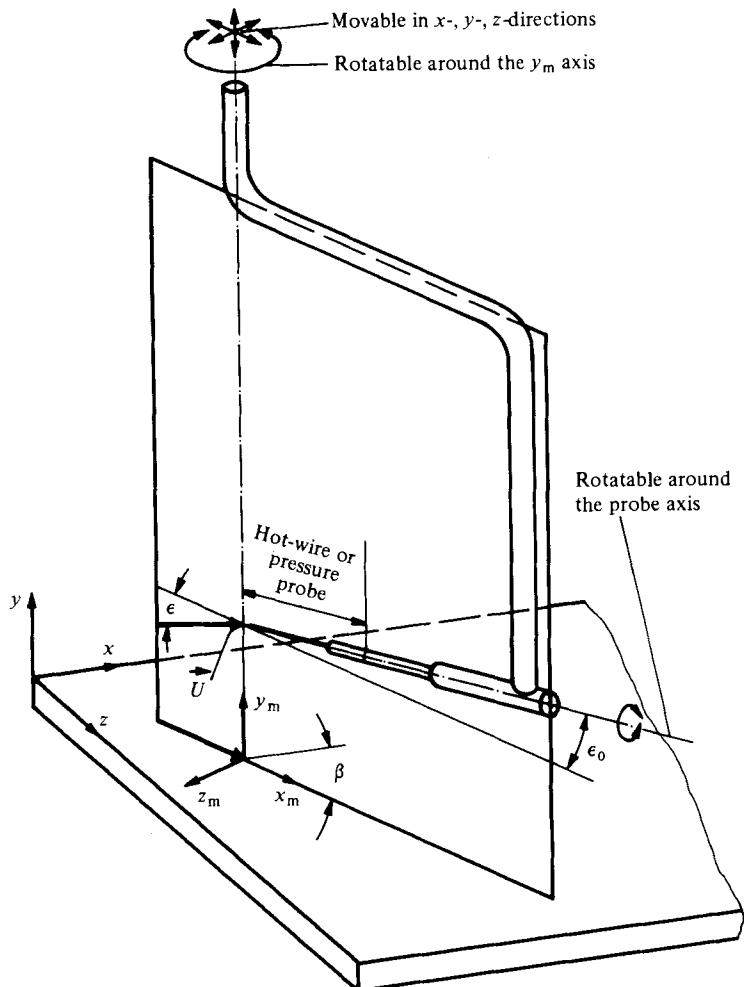
FIGURE 4. Schematic of probe support.

gauge attached to the probe support prior to the measurements (figure 5); details of the adjustments were described by Müller (1979). The accuracy in y-direction was estimated to be ± 0.05 mm for a wire lying parallel to the wall.

We used DISA 55P11 straight, single-sensor probes and 55P61 X-hot-wire probes ($5\,\mu$m platinum–tungsten wires, $l/d \simeq 240$) throughout the measurements presented in this report. The main equipment consisted out of two DISA anemometer systems, each with a 55D01 bridge, 55D10 linearizer and 55D35 r.m.s. voltmeter. Additionally, two Hewlett-Packard HP5326B timer–counters, operated as digital voltmeters, and a Thermo Systems correlator TSI 1015C were used. The upper frequency response of the hot-wire systems was adjusted to about 20 kHz, which was sufficient to resolve the highest encountered turbulent frequencies of about 7 kHz.

The method of measuring the mean velocities was described by Müller & Krause (1979), and is illustrated in figure 6. Briefly the yaw angle was measured by estimating the local mean-flow direction, rotating a single normal hot-wire lying tangential to the surface around the y-axis with angles of $\pm \Delta\beta = 45°$ in both directions and comparing

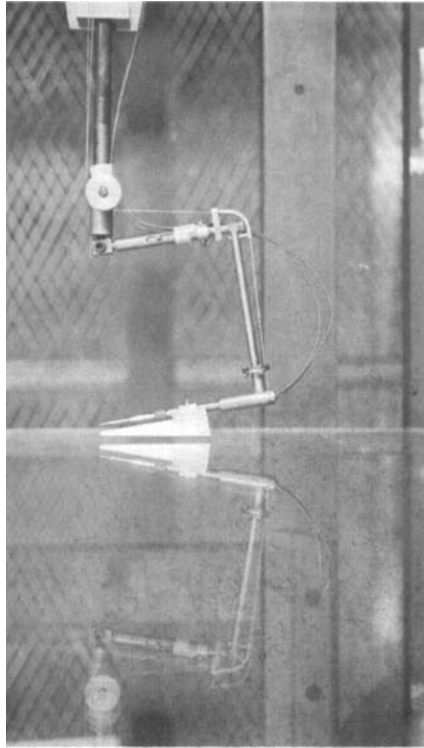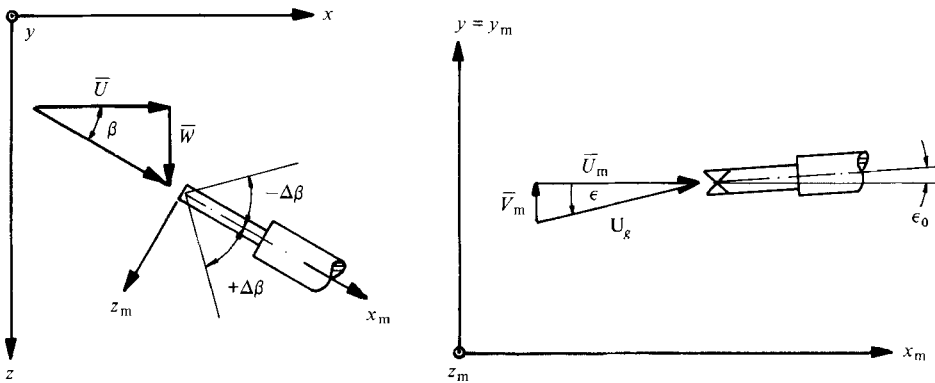FIGURE 5. Support with hot-wire probe and gauge in front
of Plexiglas plate; scale 1:6.

FIGURE 6. Measurement of yaw angle β and pitch angle ϵ of local
total-velocity vector $\mathbf{U_g}$.

the hot-wire mean voltage outputs. The line of symmetry found when the wire signals
were equal was interpreted as the mean-flow direction and defined the local measuring
co-ordinate system (x_m, y_m, z_m). This procedure, which required an average of ten
measurements at each point, was checked beforehand by means of the hot-wire cali-
bration device referred to in II. Several measurements were carried out down to
$y = 0.2$ mm from the wall, but, because of scatter, changes in yaw directions could only
be detected for $y \geqslant 0.5$ mm. The accuracy of the measured yaw angles as checked with
repeated measurements and different hot-wire probes was about $\pm 0.5°$. Errors due to

probe interferences might be inherent in the results obtained close to the wall (for a discussion see Vagt & Fernholz 1979). After measuring the yaw distribution throughout the boundary layer the magnitude of the mean velocities was measured with the probe aligned with the local yaw directions. Assuming collateral flow at the wall, the measurements were carried out as close as $y = 0.1$ mm. Then an X-hot-wire probe was inserted in the support. Because in a local (x_m, y_m, z_m)-co-ordinate system the mean-velocity component $\overline{W}_m$ vanished by definition, both remaining components $\overline{U}_m$ and $\overline{V}_m$ of the total velocity $\overline{U}_g$ could be measured with the plane of the wires being perpendicular to the wall (figure 6). The X-probe was also used for measurements of velocity fluctuations. The smallest wall distance in these measurements was $y = 1.5$ mm, though the results were expected to be impaired by mean-velocity gradients in the vicinity of the wall (see e.g. Gessner & Moller 1971; Sandborn 1976).

During the experiment great care was necessary to avoid calibration drift due to deposit of dust on the wires or to temperature changes in the free stream. Before and after the 16 r.m.s. measurements at one spatial point the hot-wire calibration with respect to the magnitude of the velocity was checked; maximum deviations of 1% of the resultant velocity were tolerated. The calibrations were carried out in the free stream behind the wind-tunnel nozzle, about 200 mm above the plate. A removable probe support was used to place the hot wires perpendicular to the flow.

2.2. *Reduction of hot-wire measurements*

Since preliminary investigations indicated that the measured turbulent stresses could be strongly influenced by experimental errors, an individual calibration of each hot wire used in the experiment was necessary. The calibrations with respect to magnitude as well as direction of the velocity vector had to be taken into account in the data reduction; for a detailed description of the procedure and calibration curves see II. The time-averaged response of a hot-wire was described by an effective cooling velocity U_c:

$$\frac{\overline{E}^2}{S^2} = U_c^2 = \overline{U_{N1}^2} + k^2 \overline{U_T^2} + h^2 \overline{U_{N2}^2}. \tag{1}$$

E was the electrical voltage related to U_c by the calibration constant S; $\overline{U_{N1}}$ and $\overline{U_T}$ were the velocity components normal and tangential to the wire in the plane of the prongs; $\overline{U_{N2}}$ was perpendicular to both. The calibration by means of a specially designed calibration device revealed that the tangential sensitivity k was not constant, as measured by Champagne, Sleicher & Wehrmann (1967), but was dependent on the magnitude and direction of the velocity vector, for examples see II or Müller & Krause (1979). This dependence required an iterative procedure to evaluate the vertical mean-velocity component $\overline{V}_m$ from the measurements. The cross-flow velocity $\overline{U}_{N2}$ encountered while rotating the hot-wire probe around its longitudinal axis was taken into account with an averaged calibrated sensitivity $h = 1.2$. In II the necessity of calibrating individually each hot wire used is demonstrated by analysing the influence of empirical cooling laws on the measured Reynolds stresses and by comparing actual results with those evaluated with the empirical law of Champagne *et al.* Since the cooling law (1) was formulated for a hot-wire fixed co-ordinate system, the velocities U_{N1}, U_T and U_{N2} were described in terms of the mean and fluctuating velocities $\overline{U}_m + u_m$, $\overline{V}_m + v_m$, w_m of the local boundary-layer co-ordinate system (x_m, y_m, z_m) (figures 4 and 6). For determining the time-averaged cooling velocity $\overline{U}_c$, (1) had to be root-
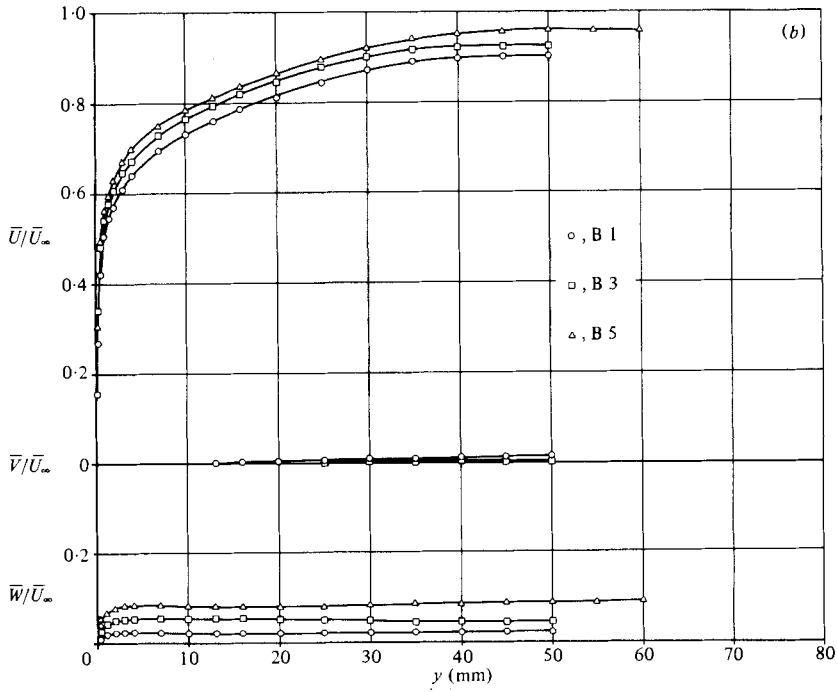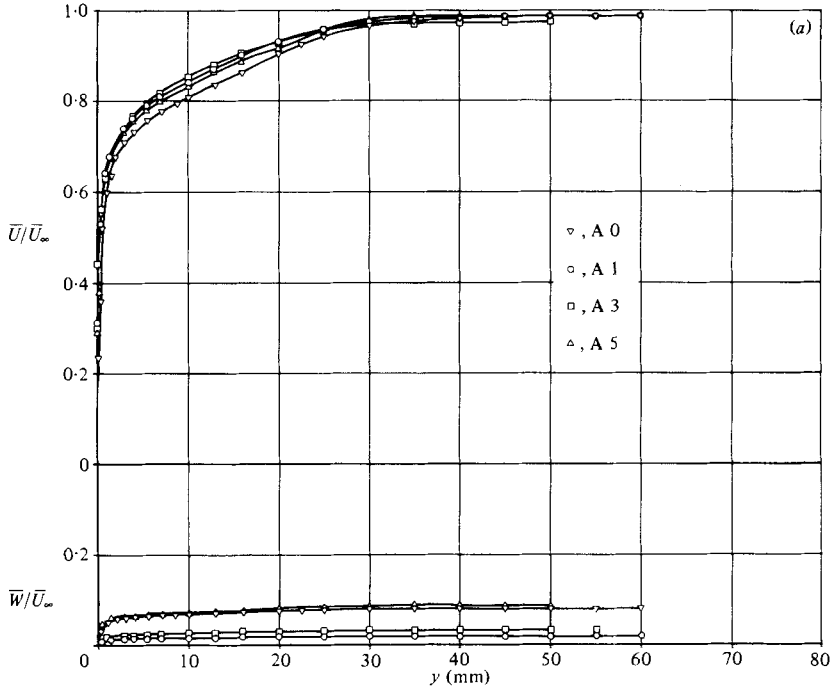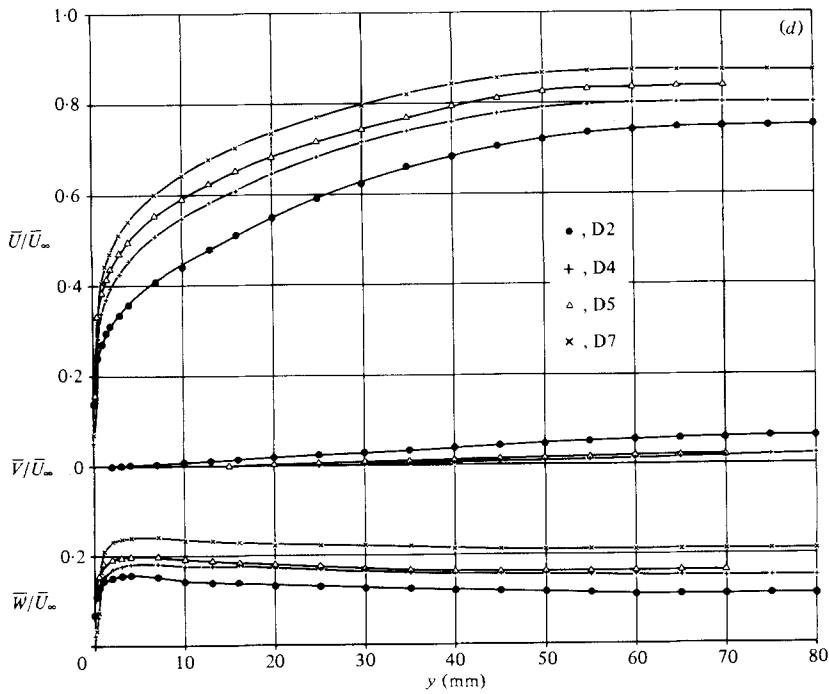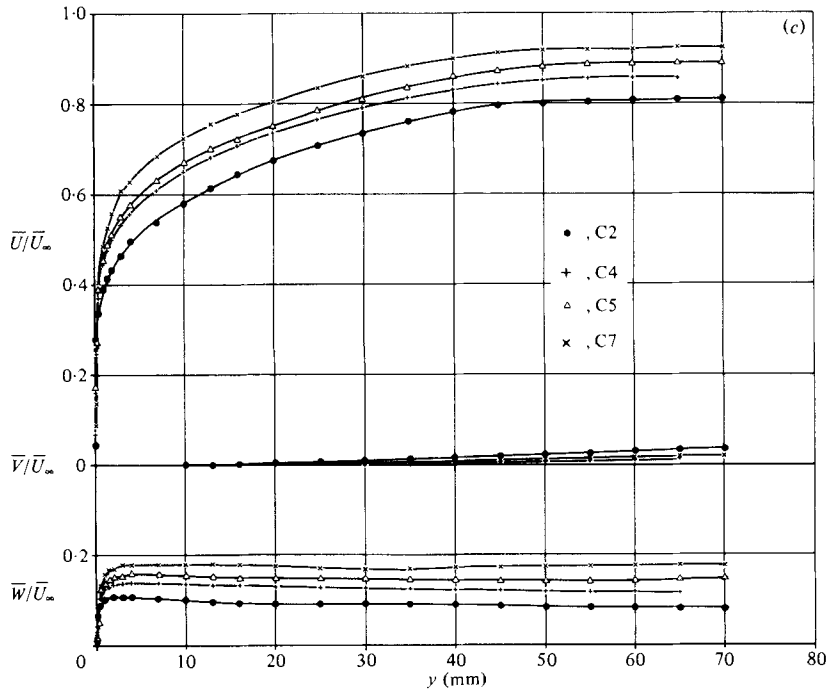
FIGURE 7 (*a*, *b*). For caption see p. 130.

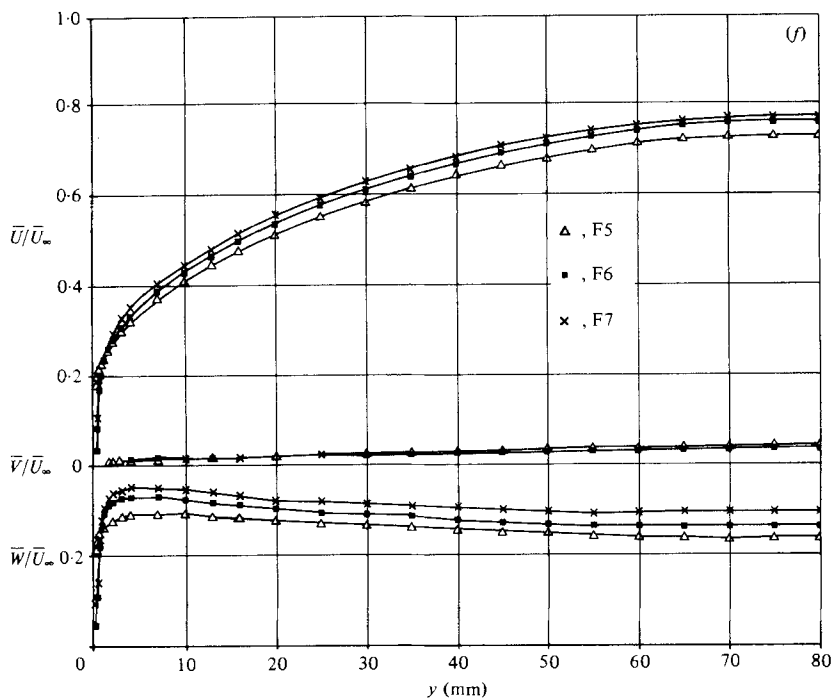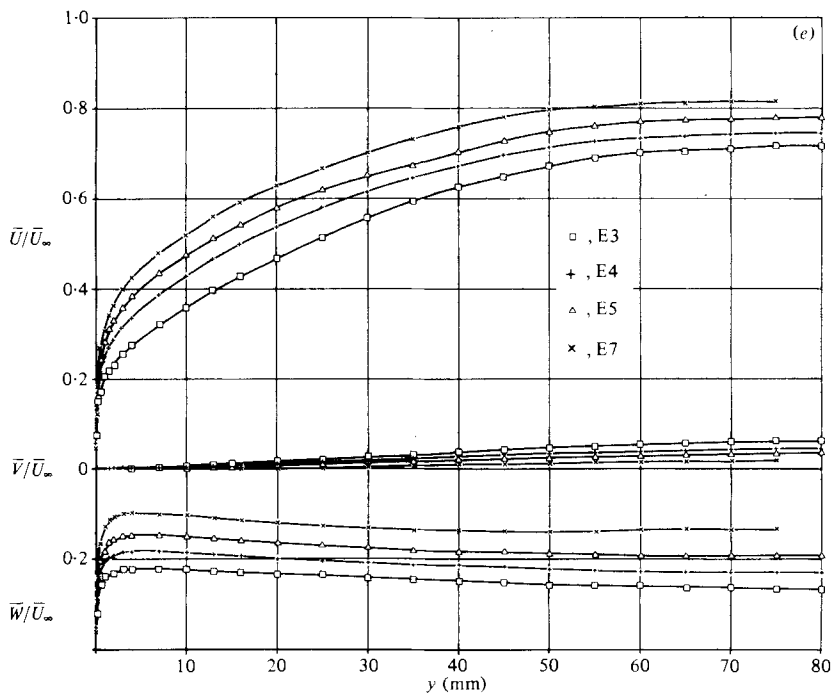FIGURE 7 (c, d). For caption see p. 130.
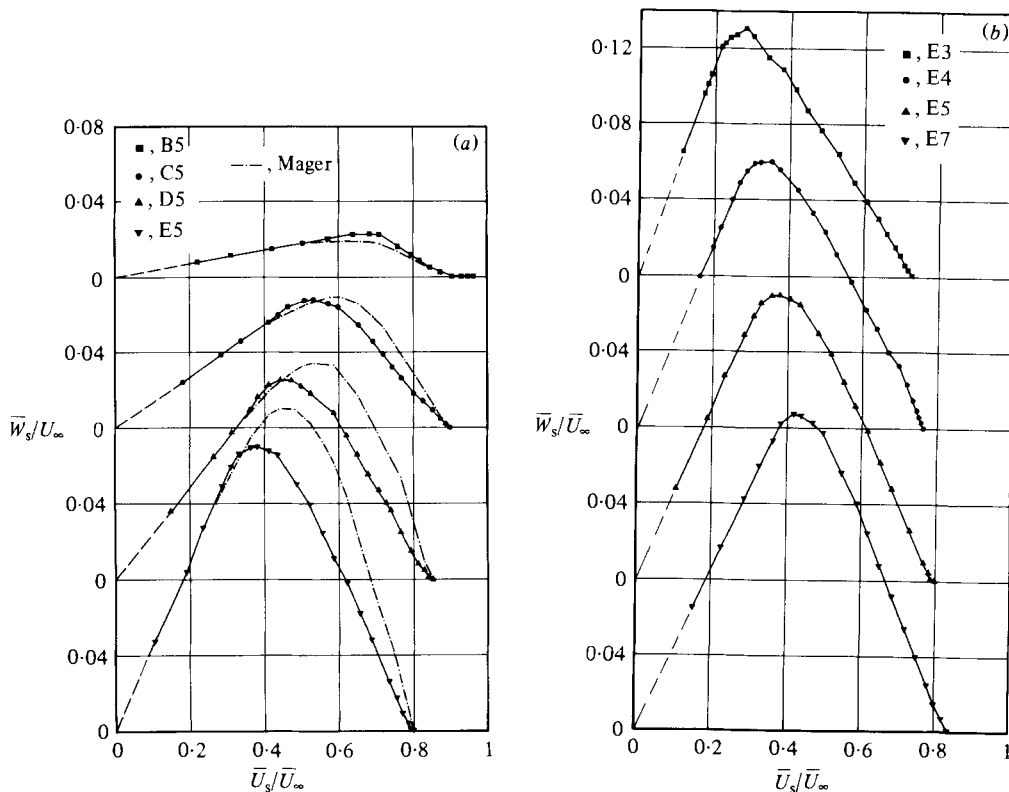
FIGURE 7. Measured mean velocities.

FIGURE 8. Polar plot of measured velocities according to Johnston (1960), and comparison with Mager's (1952) profiles.

expanded. After neglecting all terms of second and higher order, the cooling velocity corresponding to laminar flow was retained. Using this approximation for evaluating the magnitude of the total velocity vector yielded errors below 1·5%. The equations for the Reynolds stresses were obtained by squaring the fluctuating part of the instantaneous cooling velocity U_c and neglecting all correlations higher than second order. The equations for the expanded cooling velocity and those actually used for evaluating the mean velocities and the Reynolds stresses can be found in II. The applicability of the conventional linearized method for evaluating the Reynolds stress tensor was justified by additional measurements in a flow with local turbulence levels up to 35%, thus exceeding the maximum of 23 % encountered in the present investigation. All triple velocity correlations, which are usually neglected, were also measured and taken into account in the data reduction. The results as described in II revealed an increasing influence on the calculated Reynolds stresses for turbulence levels above 20% compared with the results calculated with the conventional linearized method from the same set of data.

The Reynolds stress measurements were carried out with X-hot-wire probes rotatable around the longitudinal axis. At each measuring point the r.m.s. values of both voltage fluctuations as well as those of their sum and difference were measured at four roll angles with intervals of 45°. To obtain accurate r.m.s. values the integration time was chosen to be two minutes. The Reynolds stress tensor was evaluated with

three different sets of data out of the 16 r.m.s. measurements; for details see II. The relative errors of these results were about 10%, and the errors in the shear stresses $\overline{u_m w_m}$ and $\overline{v_m w_m}$ were estimated as 10% of the local streamwise component $\overline{u_m v_m}$.

The profiles of mean velocities and Reynolds stresses discussed in §3 are unsmoothed results measured in the way outlined above.

3. Results

3.1. *Pressure distribution*

The static pressure distribution (figure 2) was measured at the boundary-layer edge by means of Prandtl tubes aligned with the local yaw direction as obtained from the hot-wire surveys; Betz and micromanometers were used. Throughout the measurements the Prandtl tubes had a fixed angle of attack of $2°$ against the wall, so that the maximum misalignment between local velocity vector and probe axis was $3°$, resulting in experimental errors up to 0.5% according to Aerodynamische Versuchsanstalt und Max-Planck-Institut für Strömungsforschung (1964). The measurements were carried out along lines of $x = $ constant, with intervals of 25 mm in the z-direction and 50 mm in the x-direction.

The order of magnitude of pressure variations in the direction normal to the wall was estimated at station E5 by evaluating all terms of the y-momentum equation from the measurements. For $y \gtrsim 13$ mm the only relevant term was $\rho\, \partial\overline{v^2}/\partial y$, yielding a maximum pressure change of 1% compared with the pressure measured at the edge of the boundary layer. In the region $y \gtrsim 13$ mm the leading terms $\rho\, \partial\overline{v^2}/\partial y$ and $\rho\, \overline{U}\, \partial\overline{V}/\partial x$ were of opposite sign, so that pressure variations in the outer layer could not be detected.

3.2. *Mean velocities*

The profiles of the measured time-averaged velocities $\overline{U}$, $\overline{V}$ and $\overline{W}$ are displayed in figure 7; each type of symbol represents a fixed z-co-ordinate. As indicated in figure 1, the measuring stations are labelled with letters for increasing x-co-ordinate and with numbers for increasing z-co-ordinate. The figures reveal the downstream development of the flow. At the measuring stations farthest upstream (column A) the flow was nearly two-dimensional, with no detectable differences between outer edge- and wall-streamline directions. The velocity component $\overline{W}$ was not zero because the wind-tunnel centre line and the x-direction did not coincide exactly. The $\overline{V}$-velocity was too small to be determined. Farther downstream, the $\overline{U}$-component was decelerated continuously with increasing x and decreasing z, i.e. increasing static pressures. Accordingly the cross flow $\overline{W}$ increased. This tendency is also displayed by the polar plots in figures 8 (a, b). Johnston (1960) has postulated a universal triangular shape for the cross-flow profiles $\overline{W_s}(\overline{U_s})$, but this could not be verified in this investigation or for example in that of Hornung & Joubert (1963). In Johnston's experiment the $\overline{W_s}$ maxima lay in the buffer layer at $y^+ \simeq 15$, Hornung & Joubert determined $y^+ (\overline{W_{s\,max}}) \simeq 150$, while here these values decreased from 215 to 175 for profiles A5 to E5 and scattered around 100 for profiles E4 to E7. The results in figure 8 (a) are compared with the cross-flow profiles of Mager (1952),

$$\frac{\overline{W_s}}{\overline{U_e}} = \frac{\overline{U_s}}{\overline{U_e}}\left(1 - \frac{y}{\delta}\right)^2 \tan\beta_w, \tag{2}$$

but these do not represent the measured data. Since possible changes of the flow direction could not be detected in the region very close to the wall, the present results for $\overline{U}_{\rm s} \to 0$ may not be regarded as a proof of collateral near-wall flow.

3.3. *Wall shear stress*

The determination of the wall shear stress was restricted to indirect measurements. At each measuring station the wall friction coefficient was obtained with a Preston tube (Preston 1954), and was derived from the velocity distribution according to Clauser (1954). During the last few years these methods, although originally developed for two-dimensional turbulent flows with zero or small pressure gradients, were successfully applied in three-dimensional flows with small or moderate adverse pressure gradients.

Wall shear stress measurements with Preston tubes rely on similarity of the inner-layer velocity profile of two-dimensional flows, and are limited to small or moderate pressure gradients (see Patel 1965). Prahlad (1968) and Krogstad (1979) applied the Preston-tube measurements in their experiments in pressure-driven three-dimensional boundary layers. Up to moderate pressure gradients they found good agreement between the profiles of the resultant time-averaged velocities and the logarithmic law of the wall, and determined the wall shear stresses with the calibrations of Patel (1965). Likewise the wall-shear-stress measurements were carried out in this investigation using a tube with 0·83 mm outside diameter and with a ratio of inner to outer diameter of 0·68. At each measuring station the tube was aligned with the mean-flow yaw direction measured closest to the wall.

The errors of the wall shear stresses measured in two-dimensional flows with adverse pressure gradients were determined by Patel as 3% or 6%, if the pressure gradient $(\nu/\rho u_\tau^3)\,(\partial p/\partial x)$ was smaller than 0·01 or 0·015 respectively; u_τ is the friction velocity $(\tau_{\rm w}/\rho)^{\frac{1}{2}}$. In the present experiment use of the resultant pressure-gradient vector in the same manner as Krogstad (1979) resulted in maximum errors for the wall shear stress lying at the upper limit given by Patel. However, if the component of the pressure gradient in wall-shear-stress direction is relevant, as assumed by Prahlad (1968), then the errors due to pressure gradients would be smaller than 3%.

Because the wall-shear-stress measurements with Preston tubes are based on the existence of a law-of-the-wall region, the universal logarithmic law of two-dimensional flows was compared with measured velocity profiles (figure 9). The broken lines were evaluated with the wall shear stresses measured with the Preston tube. As suggested by Coles (1956), the mean velocity $\overline{U}_{\rm Cl}$ in the plane spanned by the wall-shear-stress vector and the y-axis was used. At least to a good approximation the existence of a law-of-the-wall region has been verified; Krogstad and Prahlad obtained comparable results. The linear velocity distribution near the wall is also shown in figure 9; however, a comparison with the measured data is not possible owing to increasing experimental errors in this region.

In figure 9 the measured velocity profiles are compared with the law of the wall. If in turn the validity of the logarithmic law is presumed, the wall shear stresses can be deduced from the measured velocity profiles according to Clauser (1954). Pierce & Zimmermann (1973) checked the applicability of this method for three-dimensional flows. They used five different models proposed in the literature to describe the measured three-dimensional velocity profiles of Pierce & Krommenhoek (1968) and
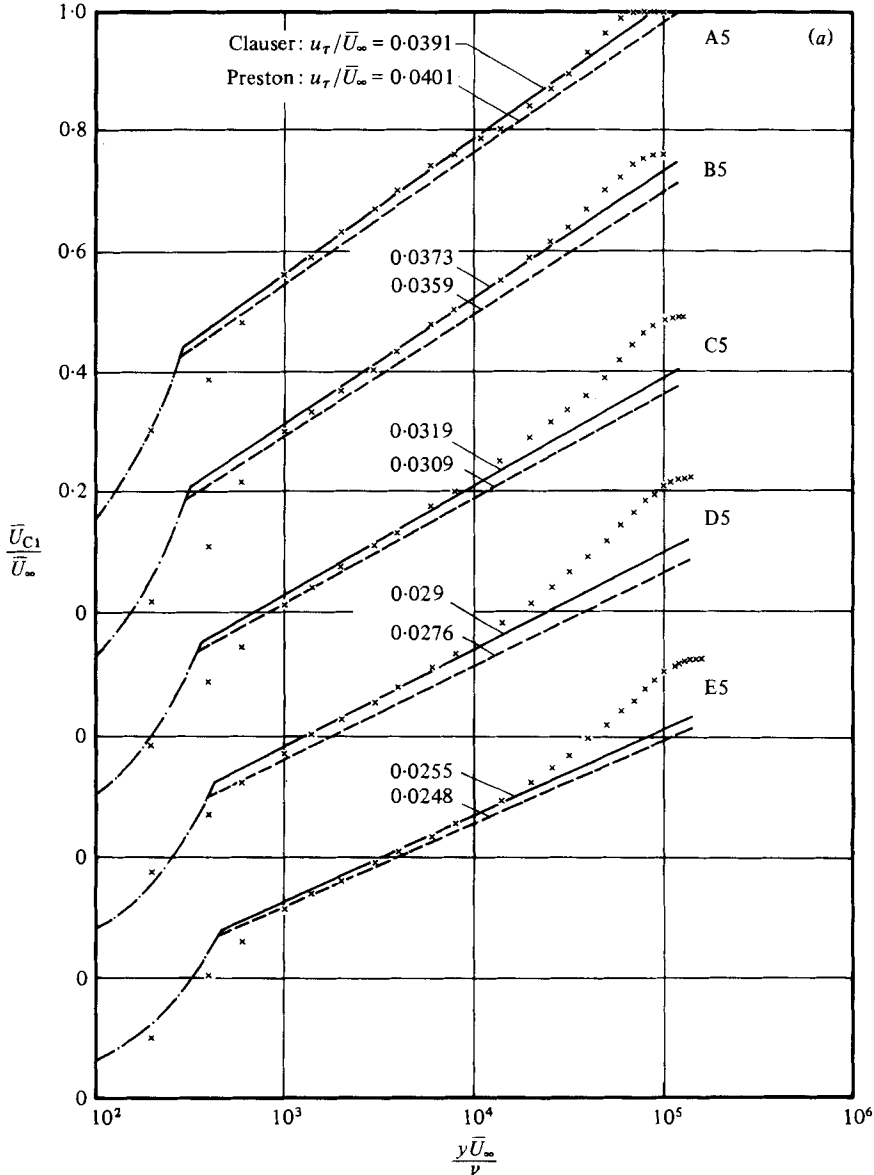
FIGURE 9 (*a*). For caption see facing page.

Prahlad (1968), and for each case they compared the wall shear stresses obtained by a Clauser chart with the data measured directly in the first investigation and obtained with Preston tubes in the latter. They achieved good agreement using the profiles $\overline{U}_{C1}(y)$ and $\overline{U}_g(y)$ as well; $\overline{U}_g$ is the mean total velocity. In the present experiment, as in that of Pierce & Zimmermann, the shear stress was determined using Schraub & Kline's (1965) procedure. The identity

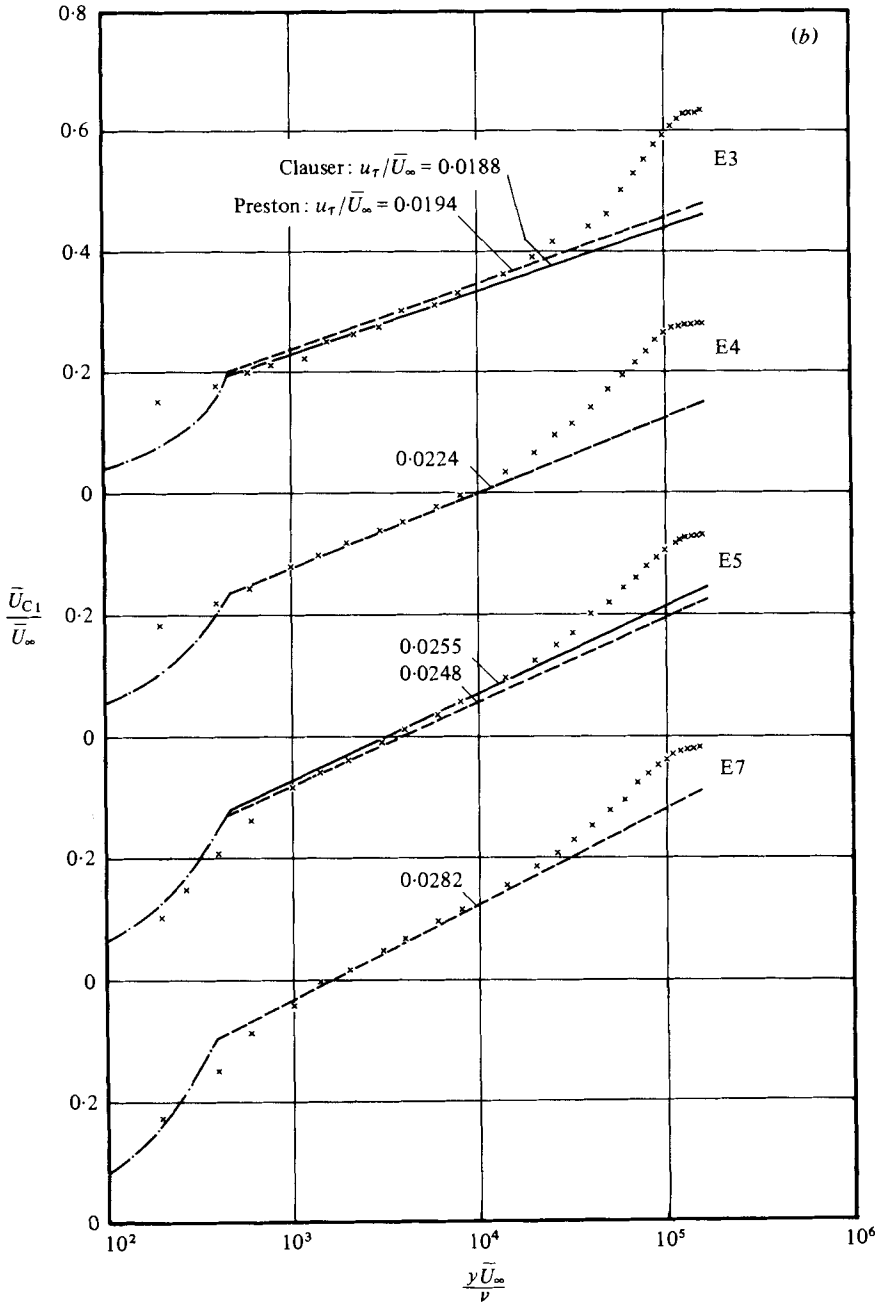$$\frac{y\overline{U}_{C1}}{\nu} = \frac{yu_\tau}{\nu}\frac{\overline{U}_{C1}}{u_\tau} = y^+u^+, \qquad (3)$$

FIGURE 9. Clauser chart. $—\cdot—\cdot—$, $\bar{U}_{C1}/\bar{U}_\infty = (u_\tau/\bar{U}_\infty)^2\, y\bar{U}_\infty/\nu$; $———$, $————$, $\bar{U}_{C1}/\bar{U}_\infty = (u_\tau/\bar{U}_\infty)\,\{5\cdot6 \log [(y\bar{U}_\infty/\nu)(u_\tau/\bar{U}_\infty)]+5\}$; $\times\times\times\times$, measurements.

together with the law of the wall $u^+ = f(y^+)$, provided an implicit equation for u^+ or u_τ respectively. Combining (3) with Spalding's (1961) extended law of the wall, which also takes into account the velocity profile of the buffer layer below the logarithmic region, yields

$$\frac{y\bar{U}_{C1}}{\nu} = u^{+2} + u^+ e^{-Ck}(e^{ku^+} - 1 - ku^+ - \tfrac{1}{2}(ku^+)^2 - \tfrac{1}{6}(ku^+)^3). \tag{4}$$
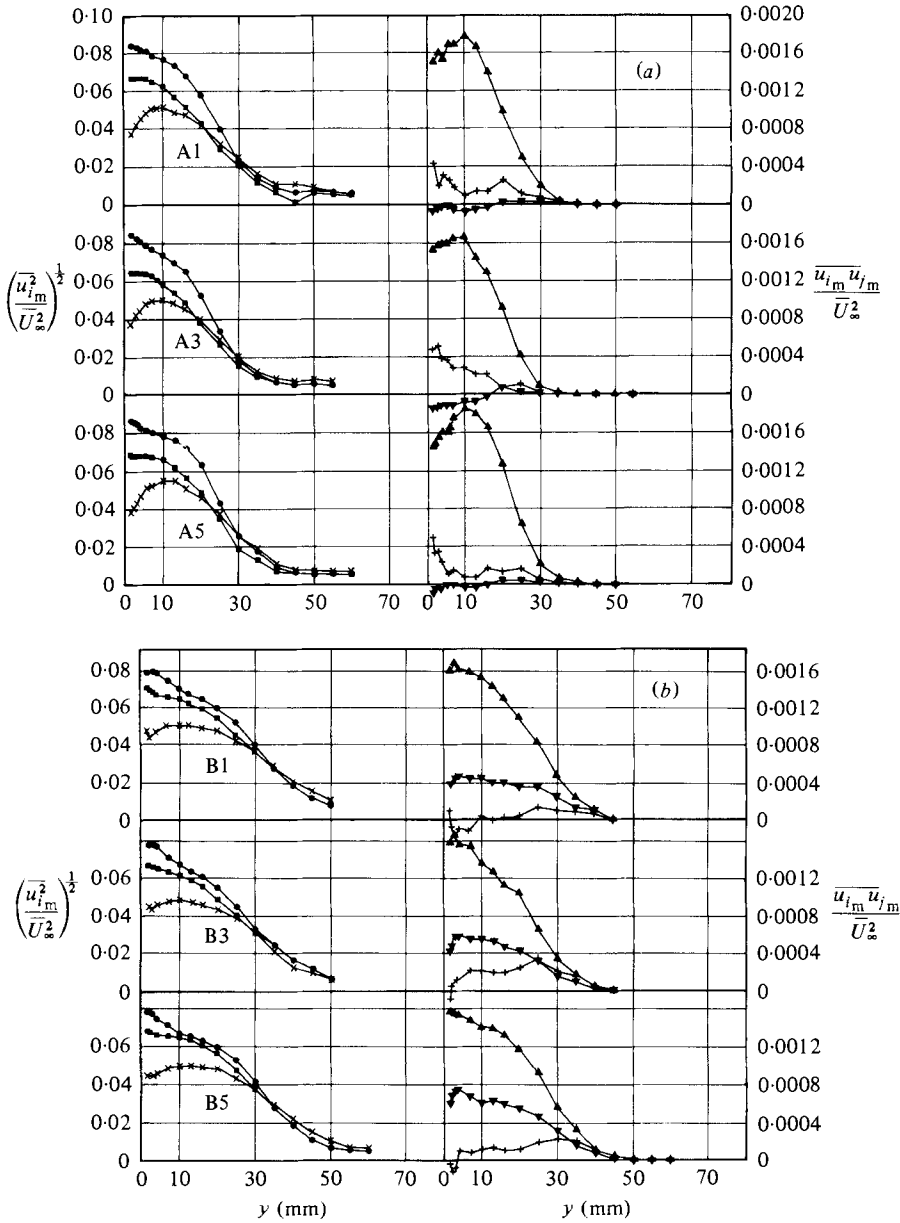
FIGURE 10 (*a*, *b*). For caption see p. 140.

According to Coles (1956) the constants $k = 0.41$ and $C = 5.0$ were used. At each spatial measuring point (4) was iteratively solved for u_τ using a computer; then the results of the logarithmic regions were averaged. The law-of-the-wall profiles obtained with these data are indicated by solid lines in figure 9. The deviations of the wall shear stresses inferred by the Clauser method compared with the results of the Preston tube measurements were within 10%.

The wall friction velocities obtained with both methods, as well as those calculated
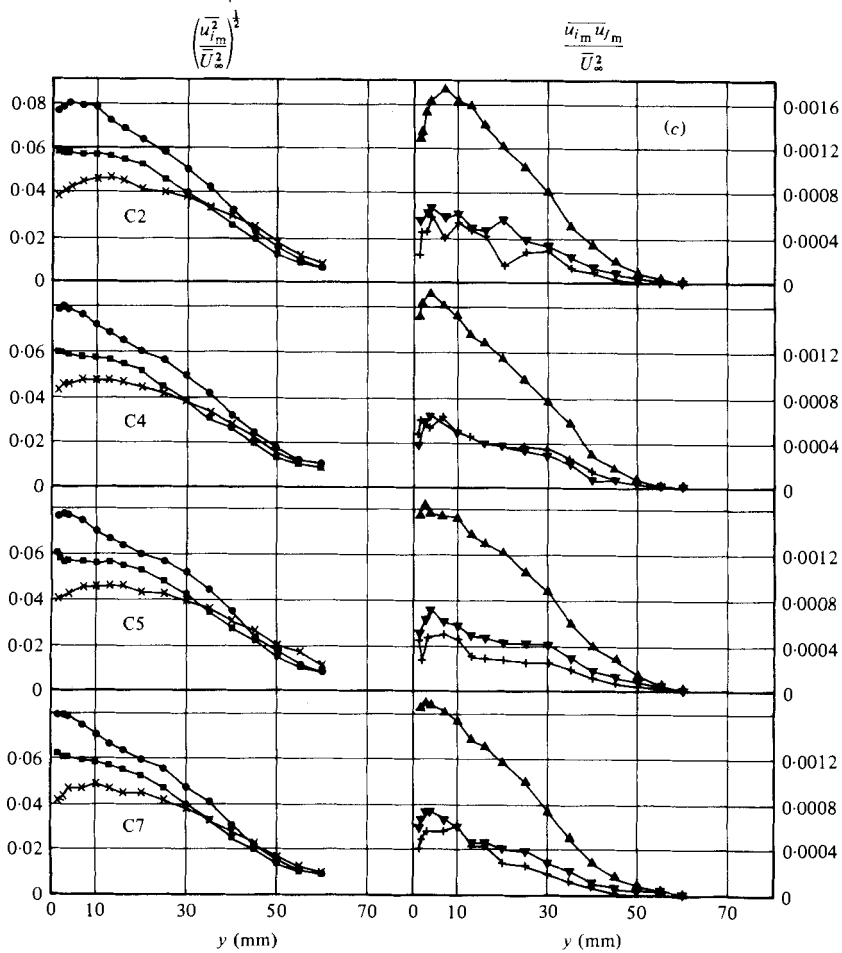
FIGURE 10(c). For caption see p. 140.

with the formula of Ludwieg & Tillmann (1949) applied to the streamwise velocity profiles, were tabulated by Müller (1979, 1980).

3.4. *Measured Reynolds stresses and comparison with closure assumptions*

The Reynolds stresses of the local measuring co-ordinate systems (x_m, y_m, z_m) are displayed in figure 10. The data are normalized with the free-stream velocity $\overline{U}_\infty$ to keep them independent of scaling variables. In each diagram all measurements at one x-co-ordinate are displayed to reveal the downstream development. The labels of the measuring stations are summarized in figure 1. The profiles of the normal stresses (figure 10a) at the stations farthest upstream have the same shape as those in a two-dimensional zero-pressure-gradient boundary layer (see e.g. Klebanoff 1955). At the outer edge they exhibit a free-stream turbulence level of 1%. The dominating shear stress $\overline{u_m v_m}$ has an unusual maximum lying away from the wall, which can perhaps be explained by a remaining influence of the tripping device at the leading edge or by measuring errors due to large mean-velocity gradients. At the stations of column B
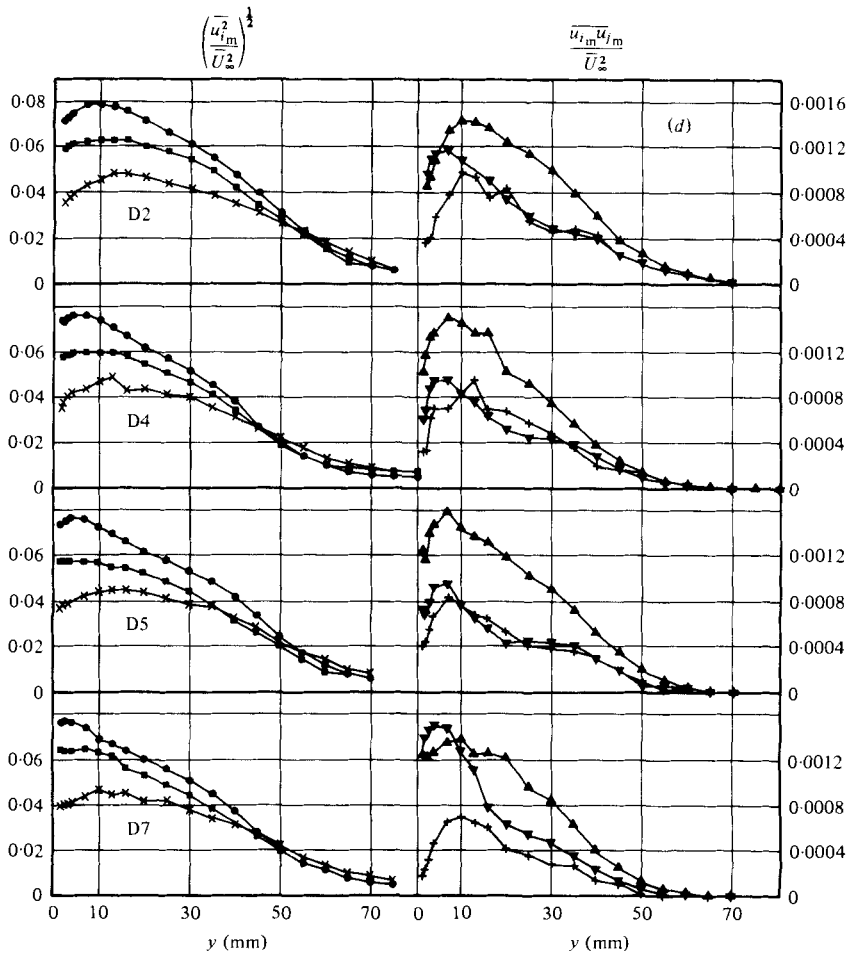
FIGURE 10(d). For caption see p. 140.

(figure 10 b) the maxima of $\overline{u_m v_m}$ lie at the wall. At column A the shear stresses $\overline{u_m w_m}$ and $\overline{v_m w_m}$ are small compared to $\overline{u_m v_m}$, but at column B the correlation $\overline{u_m w_m}$ is about one third of $\overline{u_m v_m}$ over the major part of the boundary layer. These relative large values show that even though the mean flow is nearly two-dimensional the turbulence field is not.

The following figures show that the normal stresses change slowly in downstream direction, while the profiles of the turbulent stresses $\overline{u_m v_m}$ and $\overline{v_m w_m}$ approach shapes that are characteristic for boundary layers with adverse pressure gradients; beginning at the measuring stations of column C (figure 10c), the $\overline{u_m v_m}$ maxima are shifted away from the surface according to the momentum balance near the wall $\partial \tau_{xm}/\partial y = \partial p/\partial x_m$. The $\overline{v_m w_m}$ correlations increase continuously between columns B and F, and reach the order of magnitude of $\overline{u_m v_m}$. The $\overline{u_m^2}$ component, too, shows a behaviour typical of decelerated boundary layers. With decreasing distance to separation, for example at station D2, the maxima of the $\overline{u_m^2}$ profiles are shifted away from the wall. This development can also be recognized at measuring column E (figure 10e). The results for
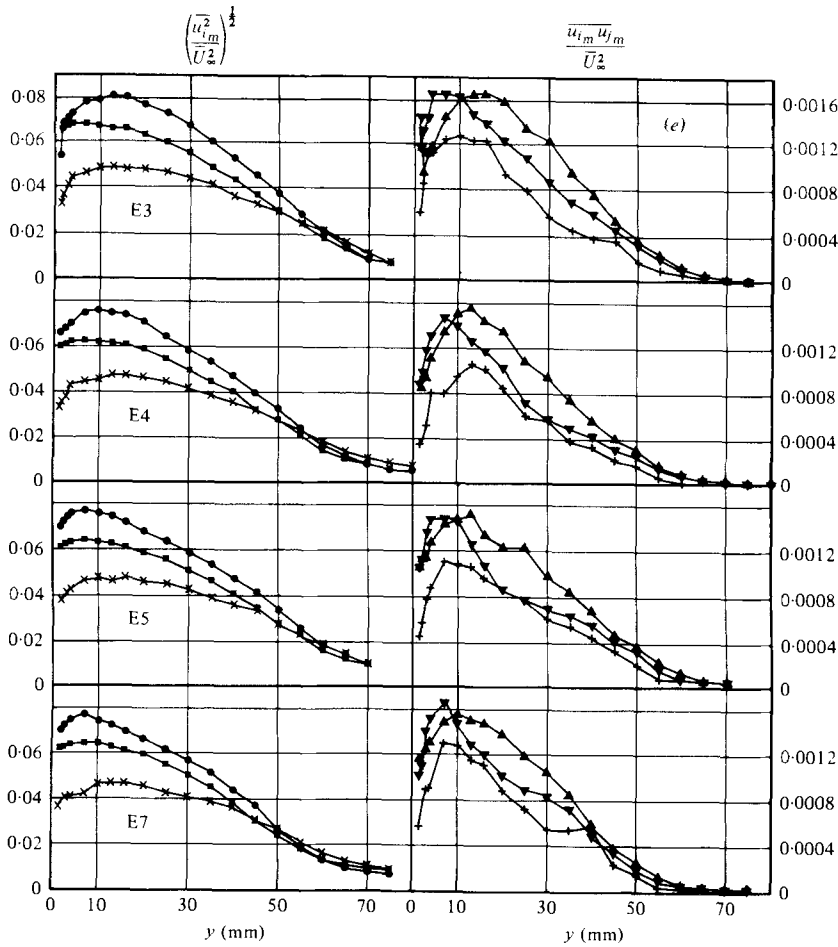
FIGURE 10(*e*). For caption see p. 140.

column F (figure 10*f*) show enlarged profiles of the $\overline{w_m^2}$ and $\overline{u_m w_m}$ correlations, the other profiles correspond to those of the preceding stations.

With the measured profiles of mean velocities and of Reynolds stresses the validity of closure assumptions with respect to the present flow field can be examined. For this purpose the measurements were smoothed by cubic splines according to Reinsch (1967). First profiles of the eddy viscosities for both tangential directions

$$\nu_{xm} = \frac{-\overline{u_m v_m}}{\partial \overline{U}_m / \partial y}, \quad \nu_{zm} = \frac{-\overline{v_m w_m}}{\partial \overline{W}_m / \partial y}, \tag{5}, (6)$$

were deduced. Those corresponding to the local streamwise directions are displayed in figure 11, normalized by the outer edge velocity $\overline{U}_e$ and the displacement thickness δ_1, which was evaluated from the streamwise velocity profile $\overline{U}_s(y)$. These diagrams as well as the following ones exhibit the downstream development of the variable under consideration by regarding the measurements of row 5 and of column E. Corresponding to the $\overline{u_m v_m}$ profiles the viscosity profiles in figure 11(*a*) have maxima at $y/\delta \simeq 0.5$, which decrease farther downstream; δ is the boundary-layer thickness.
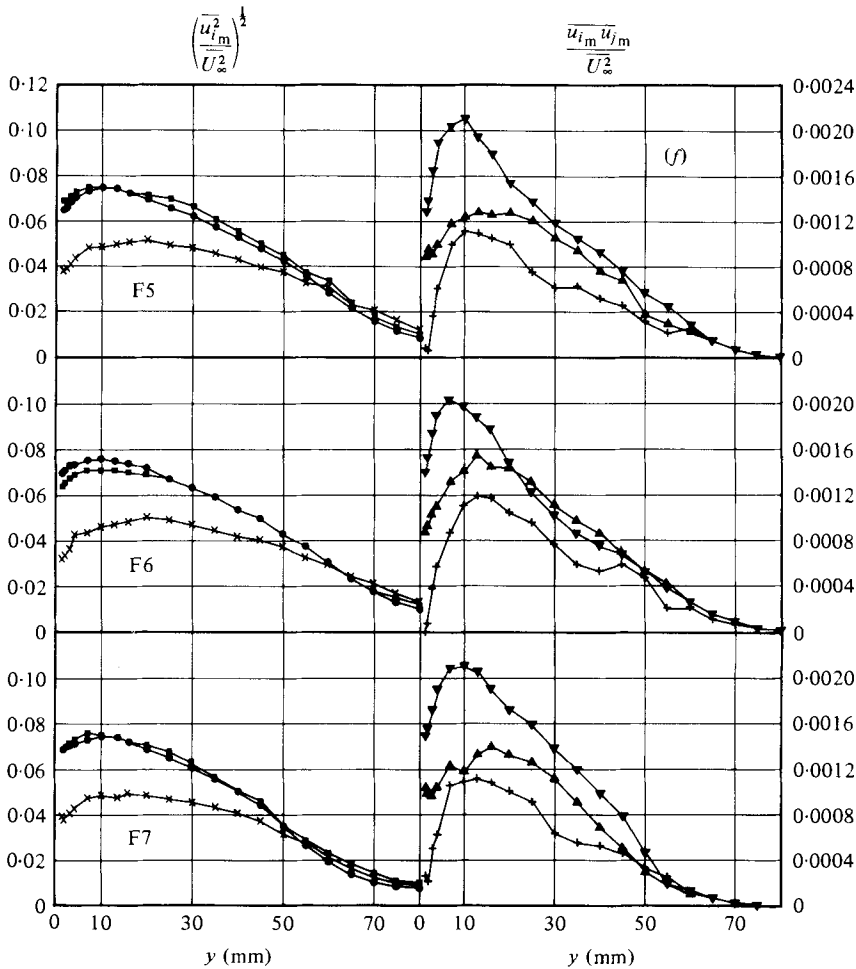
FIGURE 10 (f). Measured Reynolds stress tensor. ●, $(\overline{u_m^2})^{\frac{1}{2}}/\overline{U}_\infty$; ×, $(\overline{v_m^2})^{\frac{1}{2}}/\overline{U}_\infty$; ■, $(\overline{w_m^2})^{\frac{1}{2}}/\overline{U}_\infty$; ▲, $-\overline{u_m v_m}/\overline{U}_\infty^2$; ▼, $-\overline{u_m w_m}/\overline{U}_\infty^2$; $\overline{v_m w_m}/\overline{U}_\infty^2$.

Galbraith & Head (1975), who analysed data of two-dimensional boundary layers (Bradshaw 1967; Schubauer & Spangenberg 1960), found that the maximum non-dimensional eddy viscosity increased slightly in equilibrium boundary layers with adverse pressure gradients, while it decreased substantially in flows approaching separation. The latter tendency was evidently prevailing in the present flow. In the outer layer (figure 11 a) an approximately linear drop towards the boundary-layer edge was measured; this behaviour was also observed by Elsenaar & Boelsma in their non-separated flow. With respect to the z-direction (figure 11 b), the profiles of the dimensionless viscosity do not differ as much as those in the x-direction. These curves are similar to those determined by Bradshaw (1967) in equilibrium boundary layers.

The extension of eddy-viscosity models from two- to three-dimensional flows implies a relationship between the directions of the resultant turbulent shear stress vector and the rate-of-strain vector, which can be defined using (5) and (6):

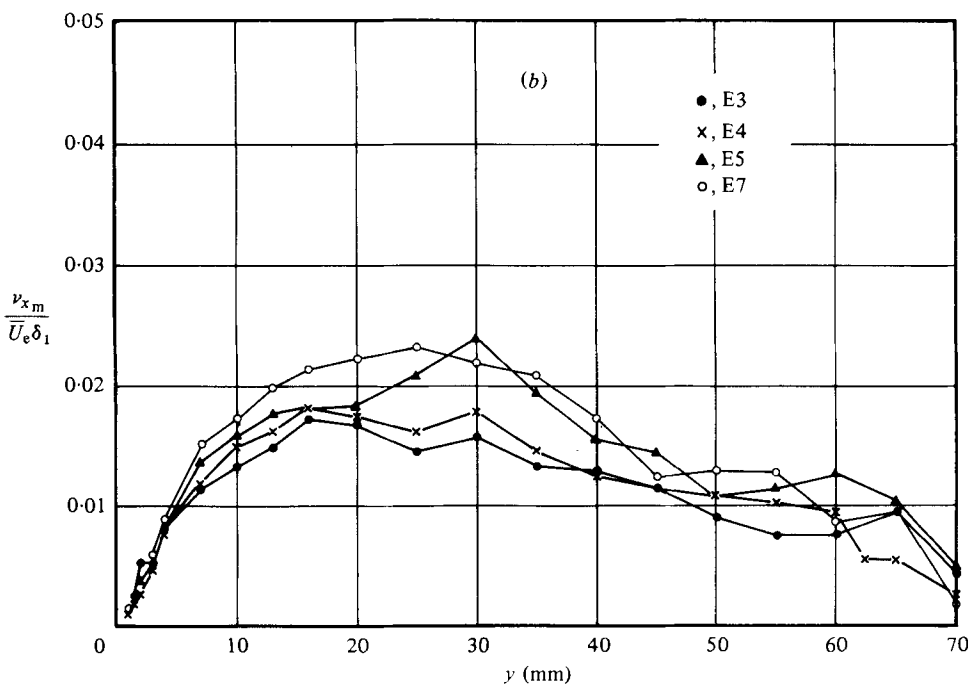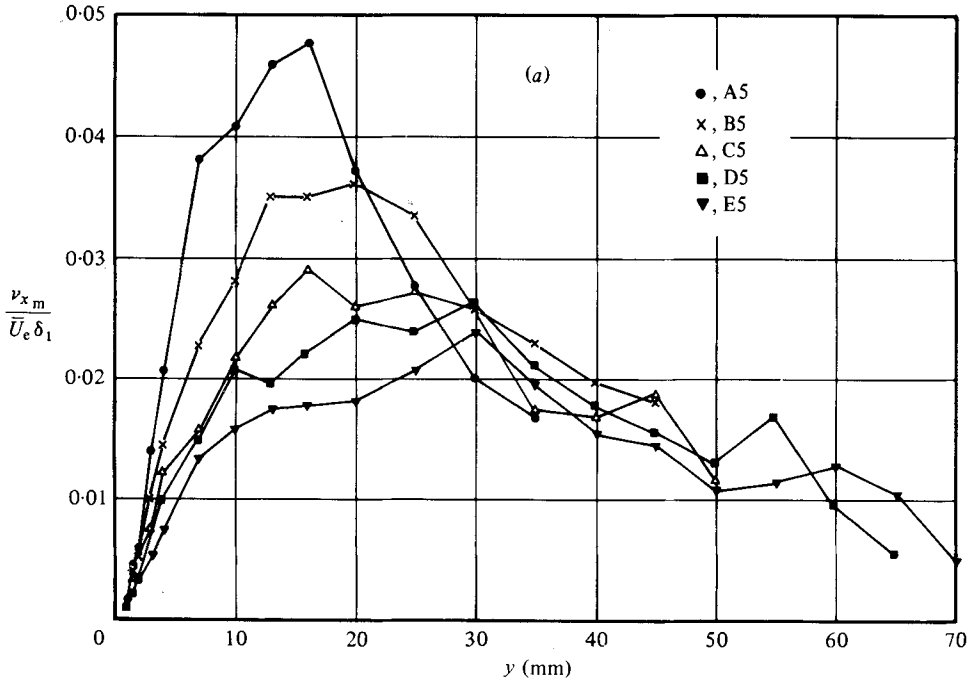$$\frac{\overline{v_m w_m}}{\overline{u_m v_m}} = \frac{\nu_{zm}}{\nu_{xm}}\frac{\partial \overline{W}_m/\partial y}{\partial \overline{U}_m/\partial y}, \tag{7}$$
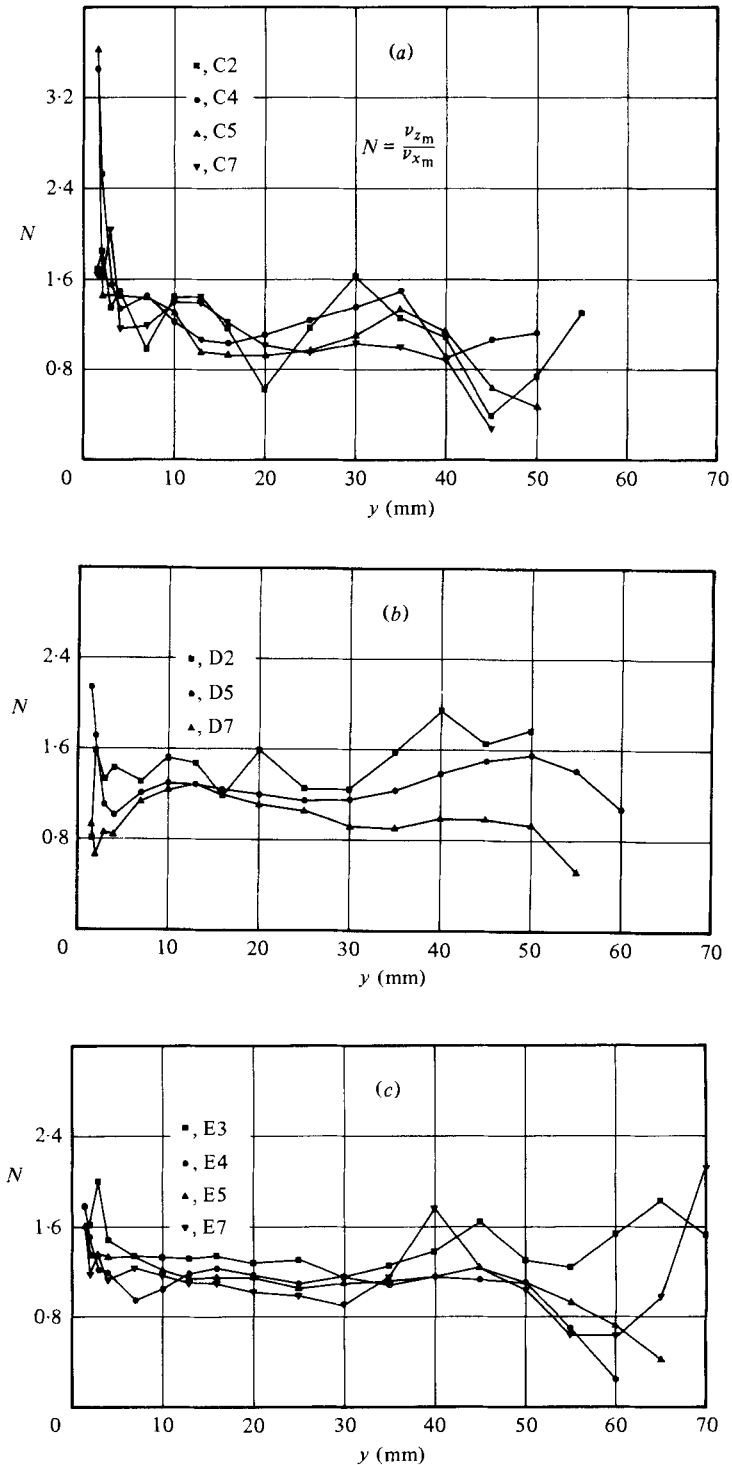
FIGURE 11. Measured eddy viscosities.

FIGURE 12. Ratio of eddy viscosities.

$$\beta_\tau = \arctan\frac{\overline{v_\mathrm{m}w_\mathrm{m}}}{\overline{u_\mathrm{m}v_\mathrm{m}}}, \tag{8}$$

$$\beta_\mathrm{G} = \arctan\frac{\partial\overline{W}_\mathrm{m}/\partial y}{\partial\overline{U}_\mathrm{m}/\partial y}. \tag{9}$$

Scalar eddy viscosities with $N = \nu_{z\mathrm{m}}/\nu_{x\mathrm{m}}$ equal to unity as well as an isotropic closure model of the pressure–strain correlation with diffusion and convection neglected (Rotta 1977) imply that both the rate-of-strain vector and the shear-stress vector have the same direction everywhere in the flow field. Generally this behaviour cannot be expected, and, as Rotta pointed out, deviations must be taken into account in prediction methods for three-dimensional flows. In the experiments of Elsenaar & Boelsma (1974), Dechow (1977) and Johnston (1970) the ratio N of the local eddy viscosities was measured to be smaller than unity, $0.5 \gtrsim N \gtrsim 0.8$, with the direction of the shear-stress vector approximately half-way between those of the rate-of-strain and the velocity vectors, $\beta_\tau \simeq 0.5\beta_\mathrm{G}$. The ratios of the eddy viscosities determined in this experiment (figure 12) suggest an approximately constant value of $N \simeq 1.2$ throughout the boundary layer corresponding to $|\beta_\tau| > |\beta_\mathrm{G}|$, if the regions close to the wall and at the outer edge are excluded because of expected insufficient accuracies of Reynolds stresses and velocity gradients. So far we do not have a physical explanation for this orientation of the shear-stress vector relative to the rate-of-strain vector. If we presume equal accuracy in this experiment and those quoted above, we must conclude that the ratio of the eddy viscosities depends strongly on the external flow conditions. It should be noted, however, that results for N are quite sensitive to experimental inaccuracies, in particular to those associated with determining the shear stress $\overline{v_\mathrm{m}w_\mathrm{m}}$; see II for a detailed error analysis.

Rotta (1979) improved the results of his three-dimensional turbulent boundary-layer calculations compared with those of the infinite-swept-wing experiment of van den Berg, Elsenaar and Boelsma by optimizing the anisotropic closure of the pressure–strain correlation. If, however, the boundary-layer equations are used for the numerical simulation of separating shear flows, the predictions might be influenced by the assumption $\partial p/\partial y = 0$; and also the usual neglect of Reynolds stress diffusion in tangential directions is not generally justified (see e.g. Simpson, Strickland & Barr 1977). In the present investigation pressure variations normal to the wall were found to be negligible. All Reynolds stress diffusion terms were estimated for station E5 and were used to check a three-dimensional version of the definition of a 'pseudo shear stress' due to Simpson *et al.* (1977):

$$-\overline{uv}_\mathrm{ps} = -\overline{uv} + \int_\infty^y \left(\frac{\partial(\overline{u^2}-\overline{v^2})}{\partial x} + \frac{\partial\overline{uw}}{\partial z}\right) dy, \tag{10}$$

$$-\overline{vw}_\mathrm{ps} = -\overline{vw} + \int_\infty^y \frac{\partial(\overline{w^2}-\overline{v^2})}{\partial z} + \frac{\partial\overline{uw}}{\partial x}\right) dy. \tag{11}$$

The gradients $\partial\overline{w^2}/\partial z$ and $\partial\overline{v^2}/\partial z$ and the spatial derivatives of $\overline{uw}$ were approximately zero. But the ratio

$$\frac{\partial(\overline{u^2}-\overline{v^2})}{\partial x} \Big/ \frac{\partial(\overline{-uv})}{\partial y} \simeq 0.1 \quad \text{for} \quad y \geqq 7\,\text{mm}$$

(Simpson *et al.* measured values as high as 0.25 close to the wall) indicates that the
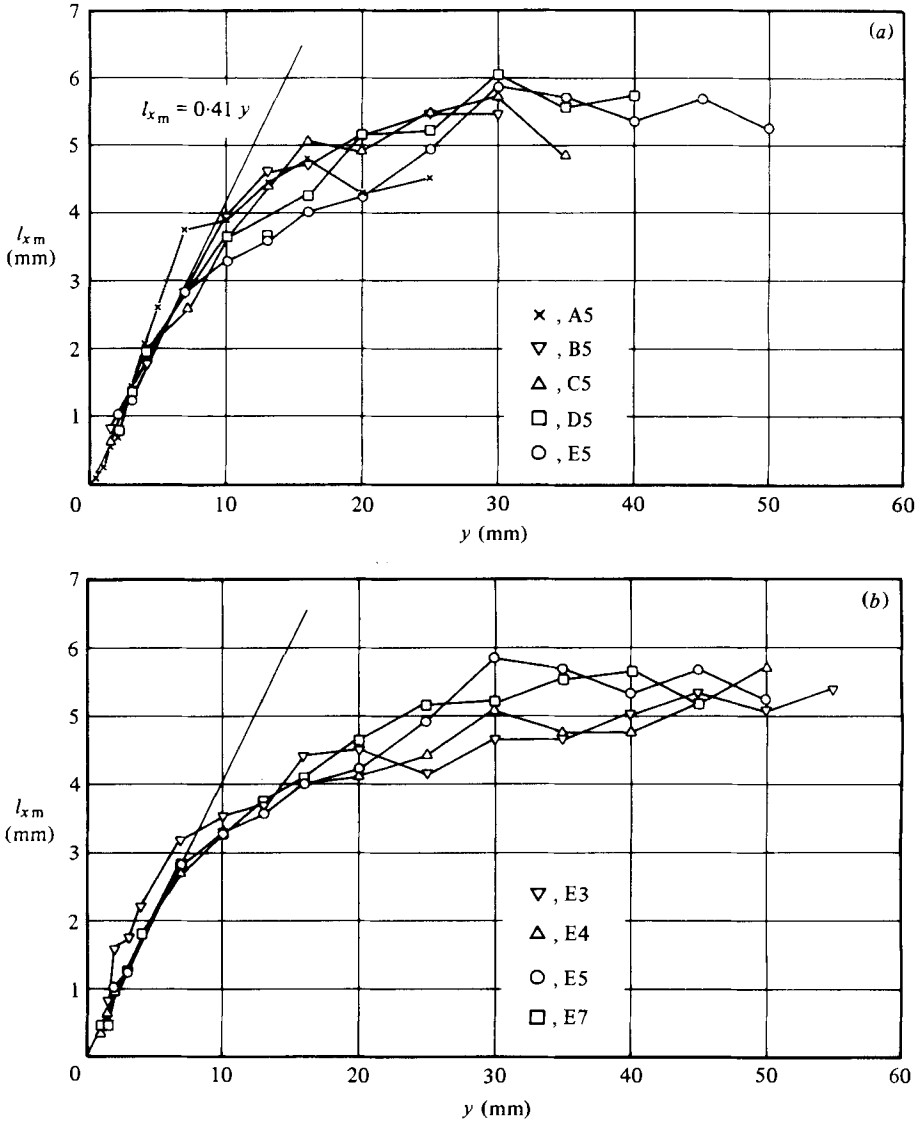
FIGURE 13. Measured mixing lengths.

pseudo shear stress $|\overline{uv}_{\mathrm{ps}}|$ is about 10 % smaller than the Reynolds shear stress $|\overline{uv}|$. This effect of the normal-stress diffusion should be taken into account in a numerical simulation of the present flow field.

Eddy viscosities are often defined in terms of algebraic mixing-length formulae (see e.g. Michel, Quémard & Durant 1969; Pletcher 1969). Though these simple closure assumptions only balance the transport equations for the Reynolds stresses with convection and diffusion terms neglected, i.e. local equilibrium, they have been applied to a great variety of flows with much success. From the measured data the mixing length $l_{x\mathrm{m}}$ for the local streamline direction was evaluated as

$$l_{x\mathrm{m}} = (-\overline{u_{\mathrm{m}} v_{\mathrm{m}}})^{\frac{1}{2}} \left\{ \left[\left(\frac{\partial \overline{U}_{\mathrm{m}}}{\partial y} \right)^2 + \left(\frac{\partial \overline{W}_{\mathrm{m}}}{\partial y} \right)^2 \right]^{\frac{1}{2}} \frac{\partial \overline{U}_{\mathrm{m}}}{\partial y} \right\}^{-0.5}. \tag{12}$$

The length scale of the cross-flow is $N^{\frac{1}{2}}$ times this value. In figures 13 (a,b) the line $l_{xm} = 0.41y$ is included for the sake of comparison.

In two-dimensional zero-pressure-gradient boundary layers inner-layer similarity intimately relates the mixing length according to $l_{xm} = ky$ (with the Kármán constant $k \simeq 0.41$) to the logarithmic law of the wall, which is derived from $\tau = \tau_w = \text{constant}$. In flows with adverse pressure gradients this assumption is violated because $\partial\tau/\partial y = \partial p/\partial x$. However, when Glowacki & Chi (1972) analysed the measurements of Bradshaw (1967), and when Galbraith & Head (1975) and Galbraith, Sjolander & Head (1977) reinvestigated the same experiments and those of the 1968 Stanford Conference (Coles & Hirst 1969), they found that in adverse-pressure-gradient flows the law of the wall approximately fits the measured velocity profiles. From this observation they concluded that the mixing length has to obey the relation $l = k(\tau/\tau_w)^{\frac{1}{2}} y$. In the experiments the 'effective Kármán constant' $k_{\text{eff}} = k(\tau/\tau_w)^{\frac{1}{2}}$ increased with adverse pressure gradients, and was as high as 0·6 for Bradshaw's strong-adverse-pressure-gradient flow. The measurements of East & Sawyer (1979) yielded similar results. In the present investigation (figure 13 a) no well-defined slope $\partial l_{xm}/\partial y$ could be found for $y \lesssim 5$ mm; values of $0.4 < k_{\text{eff}} < 0.5$ might be possible. But for $0 < y \lesssim 7$ mm ($y^+ \lesssim 400$) $l_{xm} = 0.41y$ is a reasonable approximation of the measurements except for those of station E3 (figure 13 b).

Glowacki & Chi and Galbraith *et al.* determined deviations of k_{eff} from the Kármán constant, but still they approximated the inner-layer regions of the mixing-length profiles by straight lines. Constant slopes near the wall, however, are contradictory to their definition of k_{eff}, which is a monotonically increasing function of y. Such behaviour has not yet been measured in any experiment, and would yield for example the unrealistic value $k_{\text{eff}} = 0.65$ at $y = 7$ mm of station E5.

Galbraith & Head (1975) and Galbraith *et al.* (1977) assumed that the velocity profiles of adverse-pressure-gradient flows could still be described by the universal law of the wall, and that therefore an effective Kármán constant had to be taken into account. To check this conclusion the velocity profile corresponding to $\tau \neq \tau_w$ together with $l = 0.41y$ was calculated. The measured profile of the resultant shear stress of station E5 was approximated by $\tau/\tau_w = 1 + C_1 y$, with $C_1 = 0.1$ mm^{-1}. Integration of $\partial \overline{U}_{\text{C1}}/\partial y = (\tau/\rho)^{\frac{1}{2}}/l$ yields

$$u^+ = \frac{1}{k}\left[2(1+C_2 y^+)^{\frac{1}{2}} + \ln\frac{(1+C_2 y^+)^{\frac{1}{2}} - 1}{(1+C_2 y^+)^{\frac{1}{2}} + 1}\right] + C_3, \tag{13}$$

with $C_2 = C_1 \nu/u_\tau$. Matching this profile to that of the law of the wall at station E5 for $y^+ = 15$ yields $C_3 = 18.8$. The deviations of both profiles increase with y^+, and reach 4% at $y^+ = 400$, but these small differences cannot be detected from curve-fitting the velocity measurements in the inner layer (see figure 9). The same difficulty also arises when analysing the measurements cited above. Additionally the experimental errors inherent in u^+ complicate the detection of a law-of-the-wall region. Summarizing, the measured $\overline{U}_{\text{C1}}$ – as well as the $\overline{U}_{\text{m}}$ – velocity distributions indicated logarithmic inner-layer regions, which matched the law of the wall reasonably well. Deviations from the Kármán constant $k \simeq 0.41$ could not be detected within the accuracy of the data.

Taking into account experimental scatter, the magnitudes of the mixing-length profiles displayed in figure 13 do not differ much compared with each other. This means, however, that the profiles normalized with the boundary-layer thickness δ (see
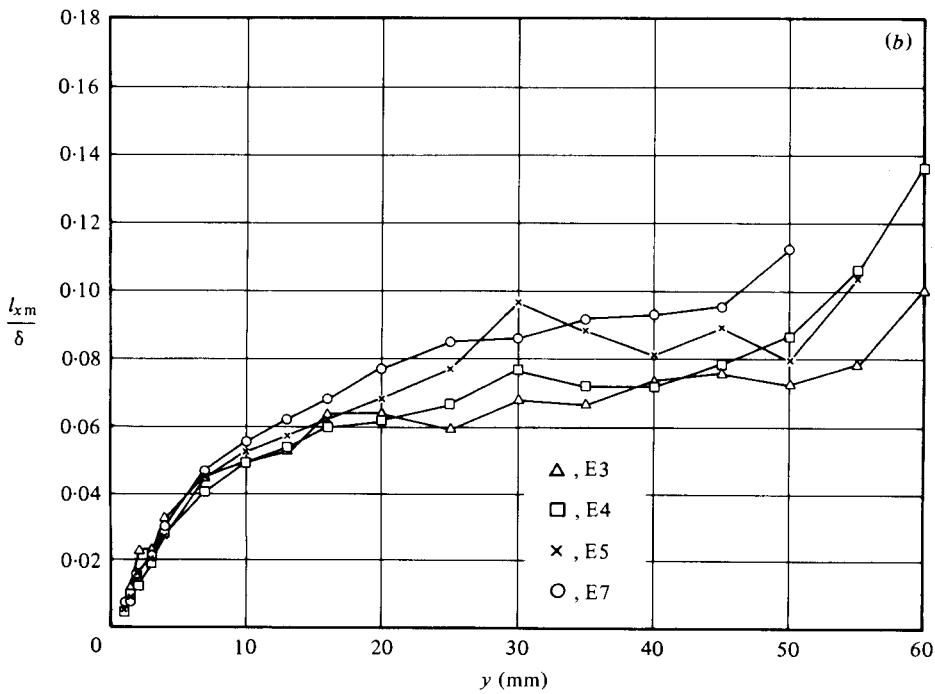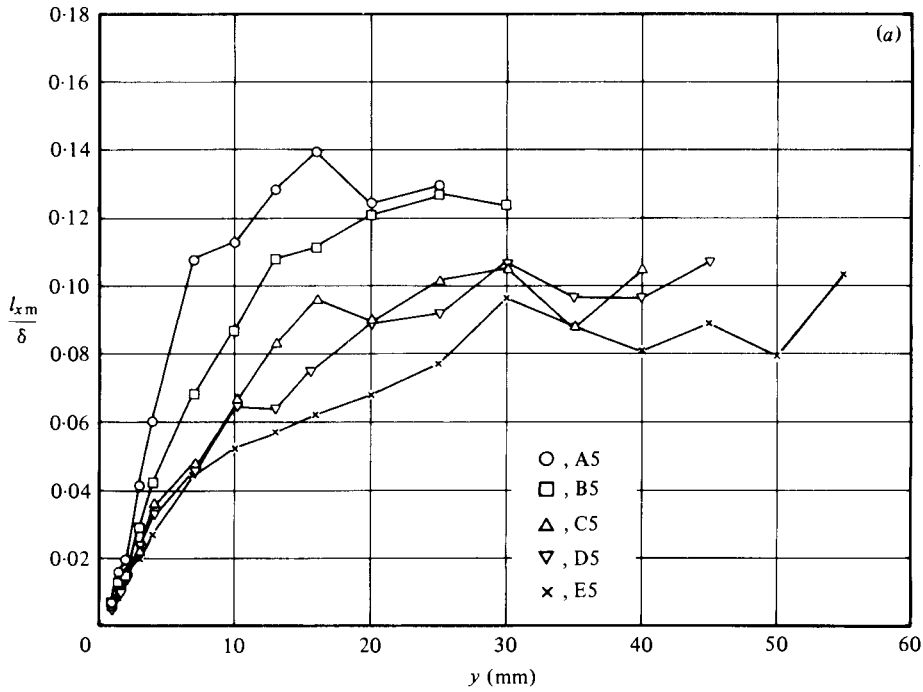
FIGURE 14. Measured mixing lengths normalized with the boundary-layer thickness.
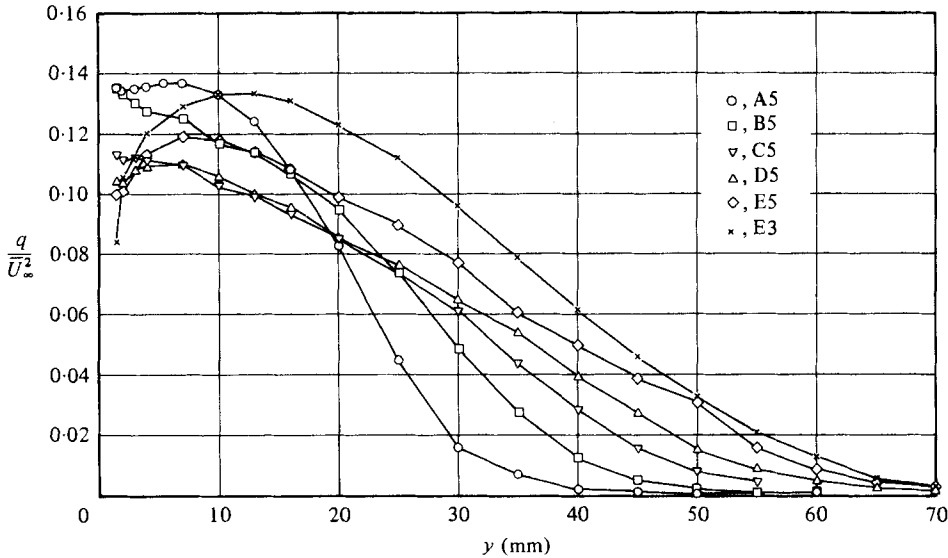
FIGURE 15. Measured turbulent kinetic energy.

figure 14) do not approach constant values in the outer layer, as assumed by most mixing-length formulae, because far downstream δ is about twice its value at the first upstream measuring stations. The decrease of the outer-layer values of l_{xm}/δ was also observed by Elsenaar & Boelsma and Dechow. The boundary-layer thickness used for normalizing l_{xm} was defined as the wall distance where the magnitude of the total velocity vector reached 0·995 of the outer-edge velocity. The values thus determined may differ from those reported by Müller & Krause (1979), which were evaluated graphically at $\overline{U}_g/U_e = 0·99$.

Finally, twice the value of the turbulent kinetic energy defined as

$$q = \overline{u^2} + \overline{v^2} + \overline{w^2} \tag{14}$$

was evaluated from the measured data and was plotted in figure 15, because the transport equation for this quantity is included in most turbulence models with one or more additional differential equations. For two-dimensional flows Bradshaw, Ferriss & Atwell (1967) converted the transport equation for q into an equation for the shear stress τ using a constant ratio of both quantities

$$a_1 = \frac{|\tau|/\rho}{q}. \tag{15}$$

This ratio was also included by Bradshaw (1971) in his closure assumptions for three-dimensional flows. The measured results of a_1 displayed in figure 16 did not reveal streamwise changes within the data scatter. In the inner layer a slight increase was observed with increasing wall distance, then a_1 was approximately 0·15, as proposed by Bradshaw *et al*. In the outer layer the magnitude of a_1 decreased slightly near the boundary-layer edge. This behaviour was mainly influenced by the shape of the turbulent shear stress profiles.

Since in adverse-pressure-gradient flows the closure assumption of Bradshaw *et al*. might be violated, Simpson *et al*. (1977) suggested that setting $a_1 F = 0·15$ would be a
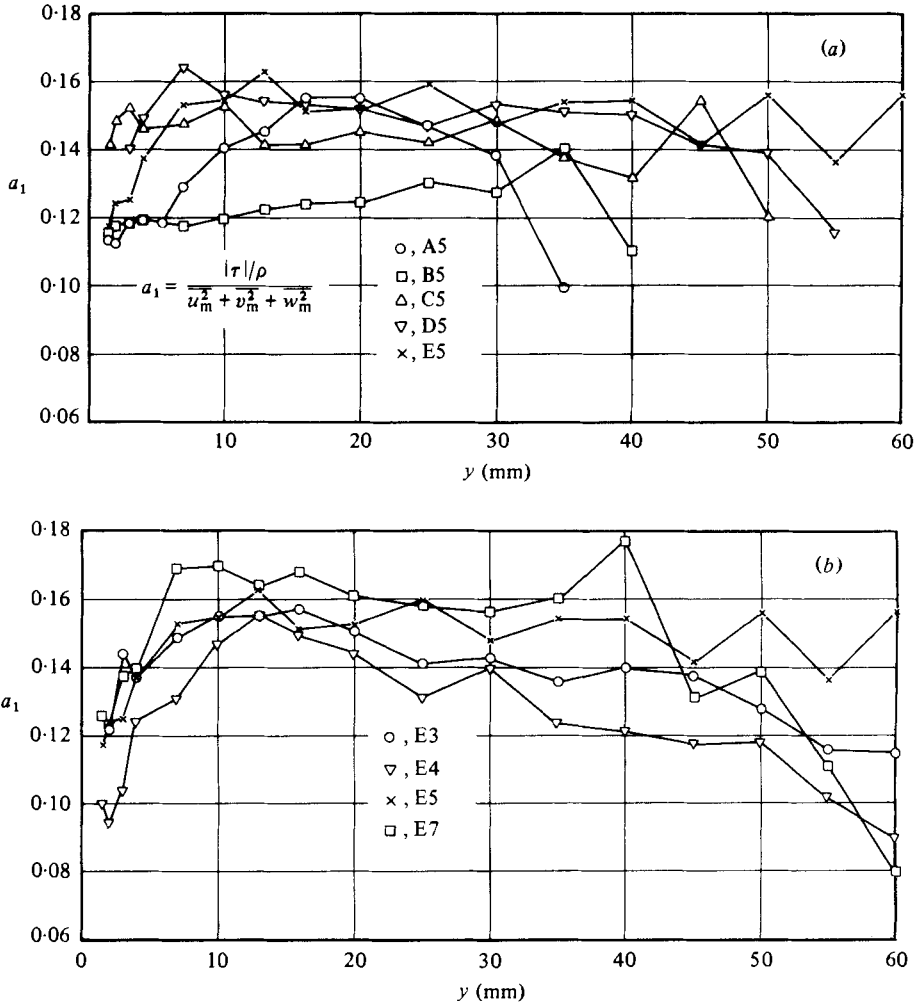
FIGURE 16. Ratio of turbulent shear stress to kinetic energy.

better approximation, where F is the ratio of total production of kinetic energy to shear production. For station E5 and $y = 10$ mm, for example, the leading production terms besides $(-\overline{uv})\,\partial\overline{U}/\partial y$ were estimated as

$$\overline{u^2}\frac{\partial\overline{U}}{\partial x}\Big/\left(-\overline{uv}\frac{\partial\overline{U}}{\partial y}\right) \simeq -0.2,\tag{16}$$

$$\overline{v^2}\frac{\partial\overline{V}}{\partial y}\Big/\left(-\overline{uv}\frac{\partial\overline{U}}{\partial y}\right) \simeq 0.1,\tag{17}$$

$$\overline{w^2}\frac{\partial\overline{W}}{\partial z}\Big/\left(-\overline{uv}\frac{\partial\overline{U}}{\partial y}\right) \simeq 0.1,\tag{18}$$

so that their sum was about zero, corresponding to $F = 1$. Therefore no conclusion concerning the correction of Simpson *et al.* was obtained. However, the magnitude of each single term above ((16)–(18)) shows that the boundary-layer approximation of

the turbulent-energy equation does not strictly hold for the downstream region of this flow.

In addition to the assumption $a_1 = \text{constant}$, Bradshaw (1971) modelled the pressure–strain correlation by introducing another constant a_3 proportional to $a_1 |\tau| / \rho \overline{v^2}$. He expected a_3 to be nearly constant for the same reasons as a_1. The present measurements indicated, however, that in the three-dimensional flow region $|\tau|(y)$ increased and then decreased more rapidly than $\overline{v^2}(y)$, and so their ratio was not constant.

4. Conclusion

The flow over a plane wall was deflected laterally by means of turning vanes. The induced pressure field, which was mapped out with a Prandtl tube, decelerated the velocity in initial flow direction and accelerated the cross-flow. Thus the boundary layer, tripped at the leading edge, developed from nearly two-dimensional to fully three-dimensional conditions. At 21 stations covering the attached flow region profiles of the time-averaged velocities and of the Reynolds stress tensor as well as the wall shear stresses were measured. Since the Reynolds stresses deduced from hot-wire measurements can be strongly affected by experimental errors, each hot wire used in the experiment was calibrated with respect to magnitude and direction of the mean-velocity vector. The influence of both an empirical and the actual hot-wire cooling law on the measured Reynolds stresses are analysed and discussed by Müller (1982). As described in the latter paper the linearized method for calculating the Reynolds stresses from the root-expanded hot-wire response equation has been found to be valid for local turbulence levels below 20%.

The main features of the flow investigated are summarized below. At all measuring stations the mean-velocity profile of the plane spanned by the wall shear-stress vector and the y-axis exhibited a logarithmic wall region, at least over the range $30 < y^+ < 500$. The measurements compared reasonably with the law of the wall of two-dimensional flows. The wall shear stresses needed for this comparison were inferred from Preston-tube measurements, as well as from Clauser charts, and agreed within 10%. The polar plots $\overline{W}_s(\overline{U}_s)$ of the streamline co-ordinate systems did not reveal a universal shape. The existence of a collateral flow region close to the wall could not be examined, because for $y < 0.5$ mm possible changes of flow directions could not be detected within the experimental scatter.

The profiles of the Reynolds stresses were characteristically shaped for boundary-layer flows with adverse pressure gradients. Excluding the measuring stations farthest upstream, i.e. column A, the turbulent stress $\overline{u_m v_m}$ in the nearly two-dimensional flow had a maximum lying at the wall, as in zero-pressure-gradient flow, while in the downstream direction the maximum was shifted away from the surface corresponding to $\partial p / \partial x > 0$. The $\overline{u_m^2}$ component, too, revealed the same behaviour, yielding large flat maxima at the stations closest to separation. The correlations $\overline{v_m^2}$ and $\overline{w_m^2}$ did not change as much as $\overline{u_m^2}$. The crosswise Reynolds stress $\overline{v_m w_m}$ increased markedly in the downstream direction, and reached the same order of magnitude as the $\overline{u_m v_m}$ correlation.

The measured data were compared with several closure assumptions. At the upstream measuring stations the eddy viscosities of the local streamwise directions had large maxima lying at about $y/\delta = 0.5$. The peaks decreased downstream, and yielded

profiles comparable to those of equilibrium flows. The ratio of the local crosswise to streamwise eddy viscosities had an average value of $1 \cdot 2$, if the near-wall and outer-edge results were excluded. This value deviated from other experiments, in which it was found to be about $0 \cdot 5$–$0 \cdot 8$. Assuming equal measuring accuracies, the results indicate a strong dependence on the external flow conditions. From the eddy viscosities the corresponding mixing lengths were calculated. In the inner region the profile of the local streamwise mixing length had the slope $k \simeq 0 \cdot 41$. Also, a velocity profile compatible with $l_{xm} = 0 \cdot 41 y$ and with $\tau + \tau_w$ was found to deviate only a few per cent from the law-of-the-wall profile, so that deviations from the Kármán constant could not be detected. Since the absolute values of the mixing lengths were nearly constant in the outer layer, these data normalized with the boundary-layer thickness δ were not constant, because δ increased rapidly in the downstream direction.

The ratio a_1 of the magnitude of the resultant turbulent shear stress to twice the value of the turbulent kinetic energy, assumed in Bradshaw's closure models to be a constant of about $0 \cdot 15$ throughout the boundary layer, was validated for the major part of the present flow field. Towards the wall a_1 decreased slightly because of a rapid drop of $|\tau|$. The proposal of Simpson *et al.* (1977) that $a_1 F = 0 \cdot 15$ would be the appropriate assumption for flows with strong adverse pressure gradients, where F is the ratio of total production of turbulent energy to shear production, was checked in the downstream part of the flow field at station E5. Three production terms besides $-\overline{uv}\,\partial \overline{U}/\partial y$ were not negligible, but their sum was approximately zero, corresponding to $F = 1$. Besides a_1, Bradshaw's turbulence model for three-dimensional flows assumes the relation $a_3 \propto |\tau|/\overline{v^2} = $ constant, which was found not to be the case in this investigation.

From the measured velocity correlations all Reynolds-stress diffusion terms were estimated from station E5 to check the assumption of negligible tangential diffusion within the boundary-layer approximations. The term $\partial(\overline{u^2} - \overline{v^2})/\partial x$ was found to be up to 10% of $\partial(-\overline{uv})/\partial y$, thus diminishing the effect of this shear stress.

All the measured data, i.e. mean velocities, Reynolds stresses, pressure distribution, wall shear stresses as well as integral thicknesses evaluated from the $\overline{U}_s$ and $\overline{W}_s$ velocity profiles were published by Müller (1979, 1980), and are available on tape.

REFERENCES

AERODYNAMISCHE VERSUCHSANSTALT UND MAX-PLANCK-INSTITUT FÜR STRÖMUNGSFORSCHUNG 1964 *Strömungsmessgeräte und Hilfseinrichtungen*, Göttingen.

BERG, B. V. D. & ELSENAAR, A. 1972 Measurements in a three-dimensional incompressible turbulent boundary layer in an adverse pressure gradient under infinite swept wing conditions. *NLR Tech. Rep.* no. 72092 U.

BERG, B. V. D., ELSENAAR, A., LINDHOUT, J. P. F. & WESSELING, P. 1975 Measurements in an incompressible three-dimensional turbulent boundary layer, under infinite swept-wing conditions, and comparison with theory. *J. Fluid Mech.* **70**, 127.

BRADSHAW, P. 1967 The turbulence structure of equilibrium boundary layers. *J. Fluid Mech.* **29**, 625.

BRADSHAW, P. 1971 Calculation of three-dimensional turbulent boundary layers. *J. Fluid Mech.* **46**, 417.

BRADSHAW, P. 1972 The understanding and prediction of turbulent flow. *Jahrbuch der Deutschen Gesellschaft für Luft- und Raumfahrt,* p. 51.

BRADSHAW, P., FERRISS, D. H. & ATWELL, N. P. 1967 Calculation of boundary-layer development using the turbulent energy equation. *J. Fluid Mech.* **28**, 593.

CHAMPAGNE, F. H., SLEICHER, C. A. & WEHRMANN, O. H. 1967 Turbulence measurements with inclined hot-wires. Part 1. Heat transfer experiments with inclined hot-wire. *J. Fluid Mech.* **28**, 153.

CHAPMAN, D. R. 1980 Trends and Pacing Items in Computational Aerodynamics. In *Proc. 7th Int. Conf. on Numerical Methods in Fluid Dynamics, Stanford University.* Lecture Notes in Physics, vol. 141, p. 1. Springer.

CLAUSER, F. H. 1954 Turbulent boundary layers in adverse pressure gradients. *J. Aero. Sci.* **21**, 91.

COLES, D. E. 1956 The law of the wake in the turbulent boundary layer. *J. Fluid Mech.* **1**, 191.

COLES, D. E. & HIRST, E. A. (eds.) 1969 *Proc. AFOSR-IFP Stanford Conf. on Computation of Turbulent Boundary Layers.* Thermoscience Division, Stanford.

DECHOW, R. 1977 Mittlere Geschwindigkeit und Reynoldsscher Spannungstensor in der dreidimensionalen turbulenten Wandgrenzschicht vor einem stehenden Zylinder. In *Strömungsmechanik und Strömungsmaschinen,* Heft 21. Mitteilungen des Instituts für Strömungslehre und Strömungsmaschinen, Univ. Karlsruhe.

DECHOW, R. & FELSCH, K. O. 1977 Measurements of the mean velocity and of the Reynolds stress tensor in a three-dimensional turbulent boundary layer induced by a cylinder standing on a flat wall. In *Proc. 1st Symp. on Turbulent Shear Flows, Pennsylvania State Univ.,* p. 9.11.

EAST, L. F. 1975 Computation for three-dimensional turbulent boundary layers. *FFA Tech. Note* AE-1211.

EAST, L. F. & HOXEY, R. P. 1969 Low-speed three-dimensional turbulent boundary layer data. Part I. *RAE Tech. Rep.* no. 69041.

EAST, L. F. & SAWYER, W. G. 1979 An investigation of the structure of equilibrium turbulent boundary layers. In *Turbulent Boundary Layers. Experiment, Theory and Modelling. AGARD Conf. Proc.* no. 271, p. 6.1.

ELSENAAR, A. & BOELSMA, S. H. 1974 Measurements of the Reynolds stress tensor in a three-dimensional turbulent boundary layer under infinite swept wing conditions. *NLR Tech. Rep.* no. 74095 U.

FANNELØP, T. K. & KROGSTAD, P. Å. 1975 Three-dimensional turbulent boundary layers in external flows: a report on EUROMECH 60. *J. Fluid Mech.* **71**, 815.

GALBRAITH, R. A. McD. & HEAD, M. R. 1975 Eddy viscosity and mixing length from measured boundary layer development. *Aero. Quart.* **26**, 133.

GALBRAITH, R. A. McD., SJOLANDER, S. & HEAD, M. R. 1977 Mixing length in the wall region of turbulent boundary layers. *Aero. Quart.* **28**, 97.

GESSNER, F. B. & MOLLER, G. L. 1971 Response behaviour of hot-wires in shear flows. *J. Fluid Mech.* **47**, 449.

GLOWACKI, W. J. & CHI, S. W. 1972 Effect of pressure gradient on mixing length for equilibrium boundary layers. *A.I.A.A. Paper* no. 72-213.

HORNUNG, H. G. & JOUBERT, P. N. 1963 The mean velocity profile in three-dimensional turbulent boundary layers. *J. Fluid Mech.* **15**, 368.

JOHNSTON, J. P. 1960 On the three-dimensional turbulent boundary layer generated by secondary flow. *Trans. A.S.M.E.* D, *J. Basic Engng* **82**, 233.

JOHNSTON, J. P. 1970 Measurements in a three-dimensional turbulent boundary layer induced by a swept, forward facing step. *J. Fluid Mech.* **42**, 823.

KLEBANOFF, P. S. 1955 Characteristics of turbulence in a boundary layer with zero pressure gradient. *NACA Rep.* no. 1247.

KRAUSE, E. 1974 Analysis of viscous flow over swept wings. *ICAS Paper* no. 74-20.

KRAUSE, E., HIRSCHEL, E. H. & BOTHMANN, TH. 1969 Die numerische Integration der Bewegungsgleichungen dreidimensionaler laminarer kompressibler Grenzschichten. *DGLR-Fachbuchreihe, Band* 3.

KRAUSE, E., HIRSCHEL, E. H. & KORDULLA, W. 1976 Fourth order 'Mehrstellen' – integration for three-dimensional turbulent boundary layers. *Comp. & Fluids* **4**, 77.

KROGSTAD, P. 1979 Investigation of a three-dimensional turbulent boundary layer driven by simple two-dimensional potential flow. *Div. Aero- and Gas Dyn., Norwegian Inst. Tech.*

LUDWIEG, H. & TILLMANN, W. 1949 Untersuchung über die Wandschubspannung in turbulenten Reibungsschichten. *Ing. Arch.* **17**, 288.

MAGER, A. 1952 Generalization of boundary layer momentum integral equations to three-dimensional flows including those of rotating systems. *NACA Rep. no.* 1067.

MICHEL, R., QUÉMARD, C. & DURANT, R. 1969 Application d'un schéma de longeur de mélange à l'étude des couches limites turbulentes d'équilibre. *ONERA Tech. Note no.* 154.

MÜLLER, U. R. 1979 Messung von Reynoldsschen Spannungen und zeitlich gemittelten Geschwindigkeiten in einer dreidimensionalen Grenzschicht mit nichtverschwindenden Druckgradienten. Dissertation, University of Aachen.

MÜLLER, U. R. 1980 Mean velocities and Reynolds stresses measured in a three-dimensional boundary layer. In *Proc. Viscous and Interacting Flow Field Effects, 5th U.S. Air Force and the Federal Republic of Germany Data Exchange Agreement Meeting. AFFDL Tech. Rep. no.* 80–3088, p. 359.

MÜLLER, U. R. 1982 On the accuracy of turbulence measurements with inclined hot wires. *J. Fluid Mech.* **118**, 155.

MÜLLER, U. R. & KRAUSE, E. 1979 Measurements of mean velocities and Reynolds stresses in an incompressible three-dimensional turbulent boundary layer. In *Proc. 2nd Symp. on Turbulent Shear Flows, Imperial College, London,* p. 15.36.

PATEL, V. C. 1965 Calibrations of the Preston tube and limitations on its use in pressure gradients. *J. Fluid Mech.* **23**, 185.

PIERCE, F. J. & DUERSON, S. H. 1975 Reynolds stress tensors in an end-wall three-dimensional channel turbulent boundary layer. *Trans. A.S.M.E.* I, *J. Fluids Engng* **97**, 618.

PIERCE, F. J. & EKZEWE, S. H. 1974 Measurements of the Reynolds stress tensor in a three-dimensional turbulent boundary layer. *Interim Tech. Rep., Virginia Polytechnic Institute.*

PIERCE, F. J. & KROMMENHOEK, D. 1968 Wall shear stress diagnostics in three-dimensional turbulent boundary layers. *Interim Tech. Rep. no.* 2, *Project 6858E, U.S. Army Research Office – Durham.*

PIERCE, F. J. & ZIMMERMANN, B. B. 1973 Wall shear stress inference from two and three-dimensional turbulent boundary layer velocity profiles. *Trans. A.S.M.E.* I, *J. Fluids Engng* **95**, 61.

PLETCHER, R. H. 1969 On a finite difference solution for the constant property turbulent boundary layer. *A.I.A.A. J.* **7**, 305.

PRAHLAD, T. S. 1968 Wall similarity in three-dimensional turbulent boundary layers. *A.I.A.A. J.* **6**, 1772.

PRESTON, J. H. 1954 The determination of turbulent skin friction by means of Pitot tubes. *J. R. Aero. Soc.* **58**, 109.

REINSCH, C. H. 1967 Smoothing by cubic splines. *Num. Math.* **10**, 177.

ROTTA, J. C. 1977 A family of turbulence models for three-dimensional thin shear layers. In *Proc. 1st Symp. on Turbulent Shear Flows, Pennsylvania State Univ.,* p. 10.27.

ROTTA, J. C. 1979 Eine theoretische Untersuchung über den Einfluss der Druckscherkorrelation auf die Entwicklung dreidimensionaler turbulenter Grenzschichten. *DFVLR-FB no.* 79–05.

SANDBORN, V. A. 1976 Effect of velocity gradients on measurements of turbulent shear stress. *A.I.A.A. J.* **14**, 400.

SCHRAUB, F. A. & KLINE, S. J. 1965 A study of the structure of the turbulent boundary layer with and without longitudinal pressure gradients. *Rep.* MD-12, *Thermosci. Div., Mech. Engng, Stanford Univ.*

SCHUBAUER, G. B. & SPANGENBERG, W. G. 1960 Forced mixing in boundary layers. *J. Fluid Mech.* **8**, 10.

SIMPSON, R. L., STRICKLAND, J. H. & BARR, P. W. 1977 Features of a separating turbulent boundary layer in the vicinity of separation. *J. Fluid Mech.* **79**, 553.

SPALDING, D. B. 1961 A single formula for the law of the wall. *Trans. A.S.M.E.* E, *J. Appl. Mech.* **83**, 455.

VAGT, J. D. & FERNHOLZ, H. H. 1979 A discussion of probe effects and improved measuring techniques in the near-wall region of an incompressible three-dimensional turbulent boundary layer. In *Turbulent Boundary Layers. Experiment, Theory and Modelling. AGARD Conf. Proc.* no. 271, p. 10.1.